2019

Evaluating the Iron Geochemistry of Terrestrial Aerosol Sources to the Subarctic Pacific Ocean

Meg Yoder
Colby College

EVALUATING THE IRON GEOCHEMISTRY OF TERRESTRIAL AEROSOL SOURCES TO THE SUBARCTIC PACIFIC OCEAN

Meg Yoder

A thesis submitted to the Faculty of the Geology Department of Colby College in fulfillment of the requirements for Honors in Geology

Waterville, Maine
April, 2019

EVALUATING THE IRON GEOCHEMISTRY OF TERRESTRIAL AEROSOL SOURCES TO THE SUBARCTIC PACIFIC OCEAN

Except where reference is made to the work of others, the work described in this thesis is my own or was completed in collaboration with my advisory committee.

Meg Yoder

Certificate of Approval

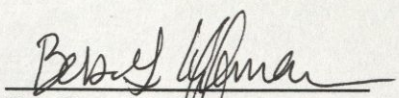

Dr. Bess Koffman
Assistant Professor of Geology
Colby College

Dr. Walter Sullivan
Associate Professor of Geology
Colby College

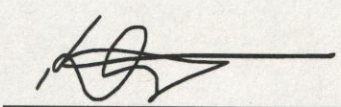

Dr. Karen Stamieszkin
Postdoctoral Fellow
Virginia Institute of Marine Science

Abstract

Wind-blown dust and volcanic ash deposited in high nutrient, low chlorophyll (HNLC) regions can fertilize phytoplankton by providing iron and other trace nutrients, in turn impacting ecosystems as well as the global carbon and nitrogen cycles. The second largest HNLC region in the world is the northeastern subarctic Pacific. Aeolian transport to this region deposits lithogenic material including desert-derived dust from Asia, glacier-derived dust from Alaska and northwestern Canada, and volcanic ash from Eurasia and North America.

This research aims to assess the geochemistry of aerosol sources to the northeastern subarctic Pacific in relation to the biological availability of iron. The samples are glacier-derived sediment and volcanic ash from Alaska, which are compared to existing published data on desert-derived sediment from Asia. The total iron content determined by complete acid digestion is compared to the iron content by chemical species determined through sequential iron extractions. The geochemistry of these samples was investigated through mineralogy using X-ray diffraction, and iron solubility assessed in Milli-Q leaching experiments.

The glacier-derived sediments have higher total iron content (average 10.9 wt. % compared to 7.46 wt. %) as well as three times higher easily reducible iron (average 2.55 wt. % compared to 0.81 wt. %) than desert-derived dust samples. Fractional iron solubility was higher in glacial sediment (average cumulative 0.261 % Fe_s) than volcanic ash (cumulative 0.060 % Fe_s). Together these results suggest that glacier-derived dust may provide the northeastern subarctic Pacific with more bioavailable iron per unit mass than either volcanic ash or desert-derived dust.

Acknowledgements

I would like to acknowledge and thank my advisor Dr. Bess Koffman for giving me the opportunity to conduct this research and for providing her guidance and expertise. I would also like to thank my committee members Dr. Bill Sullivan and Dr. Karen Stamieszkin for their feedback and advice. This project was made possible through generous support from the Buck Lab for Climate and the Environment and the Geology Department. Additional support for fieldwork was provided by the Dartmouth Society of Fellows to Dr. Koffman. Numerous people helped in completing this project and deserve thanks: Erin McConnell, Karina Graeter, Patrick Saylor, and Kristi Wallace for collecting and providing samples, Taylor Methven, Rachel Rubin, Shoshanna Geller, and Jared Fong for helping process samples in the lab, Whitney King, Lilly Naimie, and Mike Handley for helping with instrumental analysis, Zane Fields for his GIS map, and Erich Osterberg for his moral and logistical support. Finally, I would like to thank my family and friends for supporting my research and all other endeavors.

Table of Contents

1. Introduction

Aerosols in the atmosphere, such as mineral dust and volcanic ash, have major impacts on Earth systems. Earth's energy balance is altered as aerosols absorb, reflect, and scatter solar radiation. Aerosols may increase or decrease radiative forcing depending on a variety of factors including particulate size, color, and height in the atmosphere, resulting in net positive or negative effects on Earth's temperature (Penner et al. 2001; Shao et al. 2011; Li et al. 2004). Aerosols play a crucial role in cloud formation, acting as condensation nuclei for water molecules that coalesce to form droplets or crystals, and then clouds (Farmer et al. 2015). Clouds generally have a cooling effect on climate due to their high albedo, although cirrus clouds are known to trap heat (Arking 1991; Stephens 1990).

Mineral dust and volcanic ash also impact the carbon cycle, because these materials serve as nutrient sources for both marine and terrestrial ecosystems (Jickells et al. 2005; Okin et al. 2004). Trace nutrients are provided by dust and ash to high-nutrient, low-chlorophyll (HNLC) regions, which comprise over one-third of the world's surface oceans (Edwards et al. 2004; Coale et al. 1996). HNLC regions have low phytoplankton abundance relative to macronutrient availability (such as nitrate and phosphate), indicating that a trace element is likely limiting phytoplankton growth; we now know that this trace element is usually iron (Martin et al. 1988). *In situ* iron fertilization experiments have demonstrated that the addition of iron to HNLC regions can increase phytoplankton productivity (Coale et al. 1996). The original "iron hypothesis" was developed based on research in the northeastern subarctic Pacific, and iron limitation in this region continues to be an active area of research (Martin et al. 1988; Bishop et al. 2000; Serno et al. 2014; Müller et al. 2018).

Phytoplankton are key players in biological and climate systems, contributing as much to Earth's net primary productivity as terrestrial ecosystems (Field et al. 1998). Phytoplankton support a greater than five-billion-dollar fishing industry in the Gulf of Alaska (McDowell Group 2015). A decrease in phytoplankton productivity may limit productivity of species up the food chain (Stock et al. 2017). Some of the carbon biomass produced by phytoplankton is exported from the surface ocean into the deep ocean, at a rate of ~8 Pg (10^{12} kg) C per year via the biological pump. This is significant relative to the modern day concentration of atmospheric carbon (~830 Pg) and as a result, phytoplankton productivity can influence global climate (Ducklow et al. 2001; Siegel et al. 2014; Schuur et al. 2016). The results of iron fertilization experiments have been used to estimate the impact that stimulating phytoplankton blooms in HNLC regions has on atmospheric carbon. Model output shows a significant drawdown of carbon as a result of fertilization (Moore et al. 2002; Aumont and Bopp, 2006). Variable amounts of natural iron delivered via dust and ash deposition have been shown to alter phytoplankton abundance and species composition, and thus may affect how much carbon is drawn out of the atmosphere and sequestered in the deep ocean via the biological pump (Bishop et al. 2000; Goudie and Middleton, 2001; Langmann et al. 2010; Hamme et al. 2010; Sigman et al. 2010; Browning et al. 2014; Browning et al. 2015; Lambert et al. 2015; Martínez-García et al. 2014).

While the amount of dust in the atmosphere and its deposition in the ocean affect climate, dust deposition rates, in turn, are also driven by climate changes. For instance, as modern day glaciers recede, there is potential for an initial increase in dust transport as more sediment is exposed, followed by a decrease as glacial outwash plains become vegetated and glacier flour production decreases (Crusius et al. 2011). While glaciers do not directly affect Asian? desert dust sources, climate change also stands to impact this source of lithogenic material to the

northeastern subarctic Pacific. Asian mineral dust emissions are dependent on dust storm frequency, which decreased from 1960-2007, and is most significantly impacted by mean annual temperature, maximum wind speed, and average wind speed at a given location (Guan et al. 2017). The amount and rate of Asian dust transported to the northeastern subarctic Pacific may decrease, as increasing temperature has decreased wind speeds, making dust storms less frequent (Guan et al. 2017). Volcanic eruptions are less predictable than dust storms and not dependent on climate on these timescales, but nonetheless play an important role in phytoplankton fertilization (Rea 1994; Spirakis 1991).

Volcanic eruptions can cause phytoplankton blooms in HNLC regions by providing iron (Hamme et al. 2010; Browning et al. 2015; Olgun et al. 2011). It is thought that volcanic ash may provide soluble iron to the ocean more readily than either desert- or glacier-derived dust, due to the chemistry of volcanic eruptions (Browning et al. 2015). Previous work suggests that the low pH of volcanic ash clouds, which causes Fe-silicates to dissolve and reprecipitate in the ash cloud as iron-bearing salts, would result in high iron solubility (Browning et al. 2015). Leaching experiments combined with ash and dust flux estimates indicate that volcanic ash could provide similar amounts of iron to phytoplankton in the northeastern subarctic Pacific as mineral dust, although on different spatial and temporal scales (Olgun et al. 2011).

Mineral dust and ash deposited in the northeastern subarctic Pacific differ in total iron content, iron solubility, and iron speciation, all of which may impact the aerosols' relative effect on phytoplankton productivity. There are several types of lithogenic material deposited in the northeastern subarctic Pacific, including desert-derived dust from Asia, glacier-derived dust from Alaska and northwestern Canada, and volcanic ash from Eurasia and North America. Sediment cores, as well as dust trapped in ice cores, can be used as a record of the sources and fluxes of

dust and ash deposition through time (Serno et al 2014; Zdanowicz et al. 1998). Deep-ocean sediment cores show that over the past 10,000 years, volcanic ash makes up 20% of the sedimentation in the Gulf of Alaska, and up to 50% in other areas of the northeastern Pacific (Serno et al. 2014). The amount of aeolian dust transported from Alaska into the Gulf of Alaska and beyond has not been quantified from sediment cores, as researchers have yet to differentiate it from potential riverine sources (Serno et al. 2014). Researchers have begun quantifying the amount of dust transported offshore from individual dust storms using satellite data, but no estimate has been made of how much dust is deposited annually (Crusius et al 2011). In the autumn, when water levels in Alaskan rivers are low, large amounts of sediment are exposed to the air, and strong winds can transport as much as 60-160 ktons of dust into the Gulf of Alaska during a single dust storm event (Crusius et al. 2011). Constraining the composition and geochemical properties of this dust is an important step in understanding its relative importance for phytoplankton fertilization in this iron-limited region.

The bioavailability of iron from these different aerosol sources may be a result of their iron speciation, and associated physical and chemical properties. Alaskan dust is largely derived from mechanical weathering by glaciers, while much of the dust from Asian deserts is a product of chemical weathering (Gislason et al. 2009; Lu et al. 2017). The different weathering mechanisms may impact the solubility of iron; previous experiments have shown 2-3% iron solubility of glacial products leached in Milli-Q water, compared to less than 1% iron solubility in soils from arid regions (Schroth et al. 2009). Iron solubility is controlled by oxidation state and bonding environment; iron that is more easily reduced is more soluble (Schroth et al. 2009; Trapp et al. 2010). The total concentrations of dissolved and colloidal iron resulting from aerosol deposition, as well as the oxidation state of the iron, are more important controls on

phytoplankton growth than total iron content in the aerosols (Jickells et al. 2005; Wu et al. 2001; Shoenfelt et al. 2017). This means that, compared to an aerosol source with greater total iron content, a source with less iron, but more in the form of Fe (II) will likely stimulate more phytoplankton growth. Phytoplankton fertilization experiments have shown greater relief of iron limitation via the addition of glaciogenic dust than non-glaciogenic dust (Shoenfelt et al. 2017). I aim to assess whether this is a result of glacial and arid weathering mechanisms resulting in different iron speciation in glacier-derived dust and desert-derived dust.

In this project, I investigate the iron geochemistry of volcanic ash and glacier-derived dust from Alaska and the Yukon (Canada). I expect that both aerosol classes will have higher iron solubility than Asian desert-derived dust. Therefore, while a greater proportion of dust deposited in the northeastern subarctic Pacific may come from Asian dust sources, dust from local glacier-derived sources may have a greater relative impact on phytoplankton growth. By determining the iron geochemistry of modern dust and ash, I aim to constrain the relative impact on phytoplankton growth in this iron-limited region. I hypothesize that:

- Glacier-derived Alaskan dust has more "easily reducible" (and thus soluble) iron than desert-derived Asian dust (0.81 wt % average as described by Lu et al. 2017).
- Fresh volcanic ash contains the greatest percentage of soluble iron, followed by Alaskan and Yukon glacier-derived dust. Soluble iron will correspond with easily reducible and reducible iron contents.

Geochemical analyses and mineralogical assessments, as described in the methods section below, were performed to investigate these hypotheses.

2. Background

2.1 Aerosols

Small solid particles and liquid droplets (<0.001-10 μm diameters) in the atmosphere come from a variety of sources and are collectively referred to as aerosols. Aerosols, both natural and anthropogenic, have a significant impact on Earth's radiative balance through the absorption, reflection, and scattering of solar radiation, and affect the hydrologic cycle by acting as cloud condensation nuclei (Ramanathan et al. 2001; Shao et al. 2011). Aerosols with an albedo of less than ~0.85 have a net warming effect, while those with higher albedos have a net cooling effect (Penner et al. 2001). Natural aerosols include sea salt, ash and sulfates from volcanic eruptions, organic carbon, and mineral dust (Raes et al. 2000). Today, anthropogenic pollutants, such as sulfates, sulfur oxides, and black carbon particles from fossil fuel combustion also contribute to the global aerosol budget (Schoffman et al. 2016). Natural aerosol abundance in the atmosphere has been increased by human agricultural land use and deforestation, which exposes soil that was previously held in place by vegetation (Tegen et al. 2004; Guyon et al. 2005). An increase in anthropogenic aerosols can change the hydrologic cycle (Ramanathan et al. 2001) by reducing the overall amount of evaporation and precipitation worldwide, while locally increasing rainfall over deserts (Miller et al. 2004).

Aerosol particles can remain in the atmosphere for over two weeks and be transported thousands of kilometers (Prospero 1999). Volcanic sulfate aerosols can remain in the stratosphere for several months to several years after an eruption (Robock 2000; Martin 2018). Of naturally occurring aerosols, only mineral dust can be directly traced back to its source after being deposited; this is done using the radiogenic isotopic signature of the dust in comparison to potential parent source material (Banner 2004; Grousset and Biscaye 2005). Paleo-wind patterns

can be inferred using the source location of mineral dust trapped in sediment and ice cores (Grousset and Biscaye 2005). In addition, both general circulation and air-mass trajectory models have been used to predict aerosol transport and deposition patterns (Tegen and Fung 1994; Wang et al. 2009; Hyer and Chew 2010; Neff and Bertler 2015; Li et al. 2008).

In the atmosphere, aerosols are not only transported, but also chemically transformed. Atmospheric processing increases the solubility of iron borne by aerosols due to the low pH (pH 2 to 4) of the films or droplets of water that form around dust grains (Shi et al. 2012). Solubility of iron in dust is often reported as the fractional iron solubility (Fe_s), which represents the dissolved iron divided by the total dissolvable iron of the aerosol (Shi et al. 2012). The impact of acidic water on iron in mineral dust is thought to be increasing due to anthropogenic pollutants (Ito and Shi 2015). This means that, while the source sediment for dust aerosols is a first-order control on Fe speciation and solubility, residence time in the atmosphere is also an important control on iron solubility and should be taken into account in modeling studies.

Eolian dust has likely been the predominant source of iron to the subarctic Pacific during interglacial periods, while ice-rafted debris has been the primary source during glacial periods (Müller et al. 2018). While more episodic than dust deposition, volcanic ash deposition can also relieve iron deficiency in HNLC regions, though the magnitude of relief may vary based on the seawater chemistry and volcanic ash composition (Browning et al. 2015; Spirakis 1991; Capitani et al. 2018). Volcanic eruptions can produce ash plumes of iron-bearing silicate minerals and glass that are dissolved by the low pH of the plume; the dissolved components are then reprecipitated as highly soluble iron salts, but the degree to which these salts alter the amount of soluble iron in volcanic ash is unknown (Browning et al. 2015).

Aerosol deposition in the ocean does not have strictly positive impacts on phytoplankton productivity. Volcanic ash and mineral dust relieve iron limitation in HNLC regions, but they can also harm phytoplankton in some cases. Though a certain amount of trace metals are necessary for life, aerosols can elevate trace metals (such as copper) to concentrations that are toxic to some classes of phytoplankton (Mahowald 2011; Paytan et al. 2009; Mann et al. 2002). The impact of iron on phytoplankton in HNLC regions is better understood than that of other trace metals. Future research on fertilization should include geochemical characterization of other trace metals beyond iron, as well as experiments to determine trace-metal requirements.

2.2 Phytoplankton and the carbon cycle

It has long been known that the concentration of greenhouse gases in the atmosphere, such as carbon dioxide, affects global temperature (Arrhenius 1896 in Rodhe et al. 1998). The concentration of carbon dioxide (CO_2) in the surface ocean is dependent on atmospheric concentrations and vice versa, assuming equilibrium conditions (Lauderdale et al. 2016). As carbon dioxide diffuses into the ocean, it reacts with water to form carbonate (CO_3^{2-}) and bicarbonate (HCO_3^-) ions. Carbon dioxide is used by phytoplankton in photosynthesis, while bicarbonate and carbonate are used by some plankton, such as coccolithophores and foraminifera, to form tests (Giordano et al 2005; Kottmeier et al. 2014; Schiebel 2002).

There are numerous sources and sinks from which carbon fluxes into and out of the atmosphere as part of the global carbon cycle. One flux pathway that sequesters carbon dioxide from the atmosphere is known as the “biological pump”, wherein carbon dioxide that has diffused into the ocean is utilized by marine organisms and is sequestered as organic carbon in the deep ocean and carbonate in marine sediments (Longhurst et al. 1989). The biological pump is a complex network of processes, including the passive sinking of the fecal pellets from

zooplankton and gelatinous filter feeders called salps, passive sinking of particulate carbon trapped in phytoplankton tests, and active transport by daily vertical zooplankton migration (Ducklow et al 2001; Steinberg et al. 2000; Dubischar and Bathmann 1997). The biological pump is inefficient in that only a small fraction of plankton biomass, and thus carbon, is actually sequestered, with estimates of only 5-25% export from the euphotic zone (top 200 m of water column) and 1-3% actually reaching the deep sea sediments (average ocean depth 4000 m) (De La Rocha et al. 2007). While further exploration of the biological pump is beyond the scope of this project, it is important for our purposes to note that primary productivity of phytoplankton in the photic zone is proportional to the amount of carbon exported to the deep ocean (Richardson and Jackson 2007). Therefore, the iron geochemistry of dust and other influences on primary productivity play a role in the global carbon cycle.

2.3 Phytoplankton, high nutrient low chlorophyll regions, and iron fertilization

Regions of the ocean containing low chlorophyll concentrations (as a proxy for phytoplankton abundance) and high macronutrient concentrations like phosphate, nitrate, and silicate, are known as high nutrient, low chlorophyll regions (Fig. 1) (Morel et al. 1991a). Colby alumnus and oceanographer John Martin hypothesized that phytoplankton abundance in such regions could be limited by iron availability. He supported this claim by fertilizing northeastern subarctic Pacific Ocean sea water samples with iron, which resulted in phytoplankton uptake of all excess nitrate (Martin et al. 1988). Together, the Equatorial Pacific, North Pacific, and Southern Ocean cover one-third of the surface ocean and are HNLC regions (Boyd et al. 2007). Iron and other trace metals are necessary for photosynthesis, so the relatively low iron concentrations in these regions severely limit abundance. Iron is the quantitatively most important trace metal, due to its use as a redox catalyst in numerous electron transport chains

(Raven et al. 1999, Schoffman et al. 2016). Iron is also used in other phytoplankton metabolic pathways, such as nitrogen assimilation and utilization (Schoffman et al. 2016). Other trace elements needed for phytoplankton growth include manganese, cobalt, nickel, copper, molybdenum, and zinc (Morel 1999; Baeyens et al. 2011). Some of these can be co-limiting with iron in HNLC regions and are thought to be provided by volcanic eruptions (Frogner et al. 2001). The amount of each trace element varies between phytoplankton taxa, but a generalized stoichiometry of their contents is Fe ≈ Zn > Mn ≈ Ni > Co (Twining et al. 2011).

Not all iron in aerosols is biologically available to phytoplankton (Visser et al. 2003). Over 99% of iron in ocean water is bound by organic compounds called ligands (Rue and Bruland 1995). Ligands are naturally produced molecular structures that aid in iron utilization by binding insoluble Fe (III) for uptake through active transport (Benner 2011). Research shows that these ligands may be organism-specific, so certain ligand-bound – or chelated – iron complexes that aid one genus or class may limit others. For example, eukaryotes can bind iron using porphyrin, which prevents prokaryotes from utilizing it (Hutchins et al. 1999). While ligands from one taxon may limit the use of iron by another, ligands have been shown to increase the rate of dissolution of iron borne in aerosols deposited in the ocean (Aguilar-Islas et al. 2010). The impacts of ligands on iron fertilization by aerosols are complicated and not yet well understood; ongoing research is required to understand these interactions (Baker and Croot 2010).

3. Methods

3.1 Sample description

The samples used in this study include 20 glacier-derived sediment samples and two volcanic ash samples from North America (Fig. 2). The glacier-derived sediments include 18

loess and river silt samples from the Copper, Susitna, and Matanuska rivers and tributaries, covering over 320 km across the southern coast of Alaska and one lacustrine silt sample from Kluane Lake, Yukon Territory, Canada. All sediment samples were collected in the summers of 2016 and 2017. The two volcanic ash samples come from Mt. Pavlof's March 2016 eruption and Mt. Redoubt's April 2009 eruption (Smithsonian Institution Global Volcanism Program database). Both were collected during their respective eruptions and neither has been wetted, meaning any Fe-bearing salts formed during the eruptions are likely still present (Browning et al. 2015). Decisions about which samples to use for each experiment revolved around geographic and geologic breadth, with time and batch size being my limiting factors.

3.2 Geochemical processing

Geochemical analyses were performed in a class 100 laminar flow hood in a clean lab wearing proper lab attire to prevent contamination and ensure safety, including safety glasses, nitrile gloves, hair nets, and non-particulating lab coats.

The glacier-derived samples were separated by size, first using wet sieving (<63 μm grains) and then humid sedimentation following Stoke's law (<5 μm diameter), assuming spherical grains. Ultrapure water used for all experiments came from a MilliQ Integral 3 System. The <5 μm samples were then leached to remove carbonates using a pH 5 buffered acetic acid solution until non-reactive. A visible reaction occurred for loess samples that contained gastropod shells but not for other sediment samples. The <5 μm fraction represents the material most likely to be wind-transported (Prospero 1999). It is important to perform analyses specifically on the size fraction that is transported offshore since there may be geochemical and mineralogical variation based on grain size. For example, the iron content of our <5 μm samples is likely higher in finer grain sizes relative to bulk sediment, as Fe-bearing clay minerals and iron

oxides, such as hematite, goethite, and chlorite, tend to be smaller (Whitney 1975; Poulton and Raiswell 2005; Lu et al. 2017). The ash samples were purposely not exposed to water in order to preserve any Fe-bearing salts, and thus were not size-fractionated.

Complete acid digestion

Samples were acid-digested on a hotplate to determine the major- and trace-element concentrations. Samples were weighed on a Sartorius Cubis Ultra-Microbalance, which has repeatability to +/- 0.00025 mg. Approximately 100 mg of each sample was digested for 24 hours at 100˚ C in a 3:1 ratio of concentrated nitric acid to concentrated hydrofluoric acid (Optima grade). Perchloric acid was added to glacier-derived samples and fumed at 190˚ C until no organic matter visibly remained in the samples. 8N nitric acid was added to samples to remove any remaining halides, and then dried down. Samples were then brought up in 5 mL of 4N nitric acid. By drying down and then bringing up in an exact known volume, we are able to ensure a precise dilution factor for ICP-MS and ICP-OES analysis.

Mineralogy

The mineralogy of samples was determined using a Bruker D2 Powder Phaser X-ray diffractometer with a CuKα anode and goniometer radius of 141.00 mm. The <5µm grain size fraction of sediment samples were analyzed; bulk samples were used for the volcanic ash samples. Approximately 15 mg of sample was suspended in Milli-Q water, pipetted onto a silica zero-background wafer, and dried down to align clay minerals. Samples were analyzed for 2θ values from 5-30˚. Step size was 0.020˚. Peaks were identified using Bruker Diffrac.EVA software with International Center for Diffraction Data PDF-4+ 2019 database and compared to those documented in the literature (Moore and Reynolds 1989; Lu et al. 2017; Muhs et al. 2013).

3.2.3 Sequential iron extractions

Iron has varying chemical reactivity and solubility based on how it is bonded within minerals and other compounds. By following well-established protocols used in published experiments, the results are directly comparable to other studies that examine iron mineralogy and reducibility (Chester and Hughes 1967; Poulton and Canfield 2007, Lu et al. 2017). The categories of iron from these studies are exchangeable Fe(II) ions (including iron-bearing salts), "easily reducible" iron oxides (ferrihydrite and lepidicrocite), "reducible" iron oxides (goethite, hematite, and akaganéite), and iron (oxyhydr) oxides as well as iron from sheet silicate minerals (such as chlorite and biotite). These are operational definitions used to compare results with those of Lu et al. (2017) who performed similar analyses on Asian desert-derived dust samples.

The sequential extractions used 100 mg of each sample. After each extractant was added to the sample, it was sonicated and vortexed until fully suspended. After each extraction, samples were centrifuged for twenty minutes at 3900 RPM and the supernatant was collected for analysis. I used 10 mL of 1 M magnesium chloride (brought to pH 7 with 1 M sodium hydroxide) and rocked for two hours to extract exchangeable Fe(II) ions (Heron et al. 1994; Poulton and Canfield 2007). I added 10 mL of 1 M hydroxylamine–hydrochloride solution in 25% v/v acetic acid to each sample, and then placed them on a rocking table for 24 hours under dark conditions to extract "easily reducible" iron-oxides (Poulton and Canfield, 2005; Chester and Hughes 1967). I added 10 mL of sodium dithionite solution (50 g/L, buffered to pH 4.8 with acetic acid, sodium citrate, and sodium bicarbonate) to each sample, which I placed in an 80˚ C water bath for 30 minutes, shaking every five minutes, to extract 'reducible' iron-oxides (Lu et al. 2017; Poulton and Canfield 2005; Mehra and Jackson 1958). I added 3 mL of 6 N HCl at 100˚ C in Teflon beakers for 2 hours to extract iron (oxyhydr)oxides and iron from sheet silicate minerals (Poulton and Canfield 2005; Lu et al. 2017). I performed a complete digestion using the sample total

digestion procedure described above to measure residual iron left after the extractions. I calculated the sum of the extracted and residual iron from the sequential extractions to determine the mass balance relative to the total Fe from the complete acid digestions.

Solubility

To determine the iron solubility of samples, 3-4 mg of sediment (weighed on the same microbalance listed above) were placed on a 0.4-µm-pore polycarbonate filter in an acid-cleaned filtering apparatus. Researchers have often used 0.4-µm-pore filters as part of the operational definition of dissolved iron, though others discuss how iron between 0.002 µm and 0.4 µm is not actually dissolved, but rather colloidal (Wu et al. 2003). Thus, I am measuring a combination of what some consider colloids and truly dissolved Fe using this procedure. The sediment was leached with Milli-Q ultrapure water under vacuum at a rate of 250 mL in 45 seconds (Schroth et al. 2009). A total volume of 1 L was used; this was done in incremental volumes (100 ml, 150 mL, 250 mL, and 250 mL) to assess progressive solubility (based on Schroth et al.'s 2009 procedure). Samples were acidified to 3% v/v nitric acid and analyzed for iron content on a sector-field ICP-MS. Each sample was leached in triplicate.

3.3 Geochemical analysis

Inductively coupled plasma optical emission spectroscopy (ICP-OES)

Major element concentrations of the completely acid-digested samples were determined using an ICP-OES housed in the Colby College Chemistry Department. By digesting rock standards with well-characterized weight percentages, I used the slope of the known weight percentages and raw intensities of the rock standards to create a standard curve and determine weight percentages of the major elements in experimental samples.

Inductively coupled plasma mass spectroscopy (ICP-MS)

Trace element concentrations and iron concentrations from the solubility experiments were determined using a Thermo Finnigan Element II high-resolution inductively coupled plasma mass spectrometer (ICP-MS) housed at the University of Maine. We anlayzed standards made of an aliquot of the samples to account for matrix effects and differing volumes of a mixed-element standard to create a standard curve and determine trace-metal concentrations. A check standard was analyzed periodically to assess for analytical drift. The samples were run using an Elemental Scientific PFA-ST self-aspirating nebulizer with 100 µL/min uptake and a quartz cyclonic spray chamber. Sample gas flow was ~0.8mL/min with additional gas of ~0.2mL/min and RF power of ~1280. All settings were optimized during tuning before analyzing samples. Cd was analyzed in the instrument's low-resolution mode and all other elements were analyzed in the instrument's medium-resolution.

Quality assurance and control

To ensure procedural cleanliness and accuracy, I subjected a procedural blank to each step of the acid digestion, for both the first and second batch of digestions. The concentrations of a wide suite of trace elements in the two blanks, digested in two different labs (Lamont-Doherty Earth Observatory and Colby), were both low and similar to each other, suggesting that the experimental procedure contributed very little contamination to the samples.

I digested a rock standard (BCR-2) along with the samples, which I analyzed along with other rock standards (AGV-2, SDC-1, SCO-1, and another BCR-2, all previously digested by Dr. Koffman). The digested rock standards geochemically are well-characterized (USGS 2016). When operating the ICP-OES, every 4th or 5th sample (depending on the run) we ran a check. This mixture of ten samples was used to account for any "drift" (systematic increase or decrease in raw intensity) that may have occurred over the course of a given analysis run.

4. Results

Total elemental composition

The total iron content of the bulk fresh ash samples from Mt. Redoubt (AT-3982) and Mt. Pavlof (AT-3680) are 5.98 wt % and 11.9 wt % respectively. The total iron content of <5 μm sediment samples ranges from 6.89 to 14.1 wt % with a mean of 10.9 wt % and median of 10.6 wt % (Fig. 3, complete data in Table 1). The mean iron content is 9.86 wt % for loess samples and 11.52 wt % for silt samples. Reported values of bedrock from the region where the silt and loess were collected range from 2.38 to 17.0 wt % with a mean of 8.67 wt % and a median of 8.68 wt % (Greene et al. 2006 found on www.earthchem.org/petdb). This may indicate that there is an enhancement of iron in the <5 μm grain size fraction relative to the bedrock. The glacier-derived Alaskan samples have greater total iron content than the Asian sediment samples (Table 2; cite Lu here). Some of the other elements that could be beneficial (Cu, Ni, Mo) or potentially toxic (Cu) have lower abundances in the volcanic ashes compared to the loess and silt samples (Fig. 4, 5, 6). Other bioactive metals (Zn, Co, Mn) do not show any trend in amount based on the sample type (Fig. 4, 5, 6). Bioactive metals and major element concentrations of each sample can be found in Tables 3 and 4.

Sequential iron extractions

Complete data for sequential iron extractions can be found in Table 1. The average amount of iron in the form of exchangeable Fe (II) ions is 0.058 wt % for loess (n=5), 0.0097 wt % for silt (n=9), and 0.018 wt % for ash (n=2). Only 3 samples (all loess: AK2016-12, AK2016-14, and AK2016-16) have greater than 0.25% of their total iron in this form (Fig. 7). The amount of easily reducible iron is greater in all of the silt and loess samples (1.26-5.16 wt. %) than either of the volcanic ash samples (0.094 and 0.233 wt. %). Easily reducible iron makes up 9.47-

45.27% of the total iron in the glacier-derived samples, however only 1.57% and 1.96% of the total iron in the fresh ash samples is in this form (Fig. 8). There is no notable difference in amount of easily reducible iron between the silt and loess samples. The data for the Yukon silt sample is similar to the silt samples from Alaska, with the total iron and speciation data all falling within the range of Alaskan silt data.

The amount of reducible iron is between 0.078 and 1.4 wt. % (0.76-12.2% of total iron) in the glacier-derived samples. The loess samples on average contain more reducible iron than the silt samples and as a greater proportion of their total iron, with loess containing 0.67 wt. % (7.16 % of total) and silt containing 0.15 wt. % (1.33 % of total). The ash samples contain 0.012 and 0.016 wt. % reducible iron (0.10 and 0.27% of total iron), (Fig. 9). The desert sediments have high reducible iron, on average 2.29 wt. %, and the glacial sediments have high easily reducible iron, on average 2.55 wt. % (Fig. 7, Lu et al. 2017). This implies that the glacial sediments likely contain more minerals like lepidocrocite and ferrihydrite. Meanwhile, the ash samples have low amounts of both easily reducible and reducible iron. In the ash samples, the iron content within oxyhydr(oxides) and sheet silicates (2.32 and 3.09 wt. %) is similar to the lower values of glacier-derived sediments (2.65-8.23 wt. %). For the loess and silt samples, 8.55% and 12.72% of the total iron, respectively, was residual (extracted in the final step using hydrofluoric and nitric acids), compared to the ash samples which have a much higher proportion (64.25%) of their total iron in this highly refractory form.

The sum of iron extracted is similar to the total amount of iron in each sample based on the complete acid digestions (Fig. 11). The percentage of extracted iron compared to total iron ranges from 72.9 to 109.1% with a mean of 95.8% and standard deviation of 10.0%. In comparison, the percentage of extracted iron from Asian desert dust relative to total iron ranges

from 80.6 to 128.2% (Lu et al. 2017). The Asian desert dust values fit the 1:1 line more closely than the Alaskan and Yukon samples, likely due to the higher number of samples tested (Asian n=108, Alaskan and Yukon n=17), but the Alaskan samples fit the line relatively well nonetheless.

Assessment of solubility

Individual measurements of fractional iron solubility (Fe_s) range from 0.005 to 0.299%. The variability of Fe_s of glacial sediments was high within individual samples, with certain replicates of two samples (AK2016-05 and AK2016-12) releasing 2 to 200 times more soluble iron than other leaches of the same samples (Fig. 12). Sample AK2016-05 is not represented in the cumulative solubility assessment (Fig. 12) because of two extremely high replicates that distort data visualization of the other samples (Fig. 13). Four replicates of this sample were run in total due to a high measurement of the first replicate. I did this to try and constrain variability, but there is still high variability between samples.

Excluding AK2016-05, there is a positive linear relationship between cumulative Fe_s and easily reducible iron content (r^2=0.985), as well as reducible iron content (r^2=0.965). There is no relationship between cumulative Fe_s and iron contained in oxyhyr(oxides) and sheet silicates, residual iron, or total iron. There does not appear to be a systematic difference in Fe_s between glacial samples; however, the fresh ash sample (AT-3982) had the lowest average Fe_s at each interval of the total volume extracted (0.011-0.021%), (Fig. 13). The fresh ash sample also has the lowest average cumulative Fe_s (0.060 Fe_S).

Mineralogy

X-ray diffraction reveals that both the silt and loess samples from throughout the Alaska study area have similar mineral compositions, dominated by chlorite, muscovite, and quartz (Fig.

14). Plagioclase is also present in many of the samples. The peak heights are roughly proportional to the species abundance (Muhs et al. 2013). The 001, 002, 003, and 004 peaks for chlorite can be identified, but vary in total counts from sample to sample (Fig. 15). Both ash samples contain plagioclase, quartz, and K-feldspar. The ash from Mt. Pavlof (AT-3680) notably contains muscovite, while the Mt. Redoubt ash (AT-3982) does not (Fig. 16). While exact amounts of particular minerals cannot be determined for a given sample, the peak heights can be used to determine relative abundance between samples (Muhs et al. 2013).

5. Discussion

Iron geochemistry of glacier-derived vs. desert-derived dust sources

Our results demonstrate that the total iron weight percentages of the Alaskan silt and loess samples are greater than the Asian sediment samples characterized by Lu et al. 2017 (Fig. 3, Table 1). This suggests that even if there were no differences in the speciation or solubility of iron, the Alaskan dust would provide the northeastern subarctic Pacific ocean more iron per unit mass than the Asian dust, given no difference in solubility. However, we do see significant differences in the speciation and solubility of glacier-derived vs. desert-derived dust. There is over three times more easily reducible iron on average in the glacier-derived sediments (2.55 wt %) than the desert-derived sediments (0.81 wt % iron). This supports the hypothesis that glacier-derived dust contributes more soluble iron per unit mass than desert-derived dust. Ongoing research aims to quantify how much dust is deposited in the northeastern subarctic Pacific from Asian and Alaskan sources, but the lack of current estimates and high uncertainty in aerosol collection methods prevent us from estimating an accurate total easily reducible iron flux from each source (Serno et al. 2014; Landing et al. 2016; Wang et al. 2018).

While the desert-derived sediments have lower easily reducible iron, they contain more reducible iron on average (2.39 wt %) than the glacier-derived sediments (0.34 wt %) (Fig. 10). A greater ratio of iron extracted by a buffered sodium dithionite solution (Fe_2O_3, which includes reducible iron in this research) relative to total iron indicates more chemical weathering has occurred (Ding et al. 2001; Guo et al. 1998). Loess samples have higher total amounts and higher proportions of reducible iron than the silt samples, with loess averaging 0.674 wt % iron (7.16% of total iron) and silt averaging 0.153 wt. % iron (1.33% of total iron). While we did not radiocarbon date the tree stumps exposed in the Chitina loess outcrop, other investigators have dated the Chitina loess (samples AK2016-11 through AK2016-16 are Chitina loess) is estimated to be 1000 to 9100 calibrated years B.P. (Muhs et al. 2013). Higher reducible iron in the loess is likely the result of various environmental leaching and soil formation processes that impact iron geochemistry, as the loess is much older than the silt (Lindsay 1991). The samples from the Chitina loess have increasing reducible iron with depth (older samples have lower ID numbers), suggesting that reducible iron increases through time exposed at the surface.

The XRD analysis supports the accuracy of data from the boiling hydrochloric acid step of the sequential iron extractions, which targeted Fe-bearing sheet silicates including chlorite. High 002 and 004 basal reflections of chlorite indicate iron-richness (Muhs et al. 2013). Samples that yield high 002 and 004 chlorite peaks are the ones that have large proportions of their iron in the form of oxyhyr(oxides) and Fe-bearing sheet silicates (AK2016-03), while low 002 and 004 peaks coincide with low oxyhyr(oxides) and Fe-bearing sheet silicate content (AK2016-12). The mica present in the Mt. Pavlof sample is likely not an iron bearing form, as the Mt. Pavlof sample has lower HCl-extracted iron than the Mt. Redoubt sample. Further exploration of the mineralogy may aid in understanding what drives iron speciation in these samples.

Solubility of iron in glacier-derived dust

The iron solubility of the glacier-derived samples is somewhat lower than, but similar to, previously reported values, both in µg soluble Fe/g material and Fe_s. Schroth et al. (2009) report 121 (±31) and 64 (±17) µg soluble Fe/g material for their first 250 mL leach of two different Alaskan glacier-derived samples from similar locations (Matanuska and Kuskulana glacier flour). The glacier-derived samples (excluding AK2016-05) yielded 86 (± 122.4), 49 (±5.60), and 21 (±4.89) µg soluble Fe/g material for the first 250 mL of leachate. The variability between replicates may account for some of the difference between our experimental values and Schroth et al.'s previously reported values. Compared to leaching values for volcanic ash and Chinese desert sediments (and 8.1 µg/L) the glacier-derived samples from both studied are comparable. The Fe_s of previously reported glacial samples are similar to the values in this report (ranging from ~0.3 to ~0.9 % Fe_s for 750 mL, compared to 0.21 to 0.43 % Fe_s for our samples), (Schroth et al. 2009).

Volcanic Ash

The total iron content measurements of the ash samples are close to reported values, with the Redoubt sample at 5.98 wt % compared to ~5.5 to ~6.5 wt % for reported values, and the Pavlof sample at 11.9% compared to ~8 to ~9.5 wt. % (www.earthchem.org/petdb). I expected that the fresh volcanic ash would have greater fractional iron solubility than the glacier-derived sediments, but found that the fresh volcanic ash actually has less lower soluble iron than all of the glacial dust samples. The ash samples also have the lowest amounts of easily reducible and reducible iron, which may account for why the solubility was so low (more reducible forms of iron tend to be more soluble). The Fe-bearing salts, which I expected to dissolve most readily, may be represented in the sequential iron extractions as exchangeable Fe (II) ions (Browning et

al. 2015). Though the Fe-bearing salts may be present, since they account for such a low fraction of the total iron content of the ash (less than 1%), these salts likely do not compensate for the lack of easily reducible and reducible iron. The results fall at the low end of a previously reported range of Fe_s for fresh volcanic ash samples, with 0.011-0.021 % Fe_s for our samples compared to 0.007-0.1 % Fe_s (Olgun et al. 2011). While this research also reports Fe_s, different experimental and analytical techniques were used for the Olgun et al. 2011 analysis, making my results less comparable. A decrease in Fe_s of ash samples that have been stored for prolonged periods of time prior to analysis (10-20 years) has been shown to occur and may be due to the instability of Fe-bearing salts (Olgun et al. 2011). The sample I leached was 10 years old, leaching of the other sample, that is only 3 years old, may test this claim.

Volcanic ash can cause phytoplankton blooms; the limiting nutrient provided to HNLC regions is most often iron, but other trace metals can impact growth. The possibility of some trace metals having a negative (i.e., toxic) impact while iron has a positive one is unlikely for these samples. Leaching data show that the copper concentrations are too low to have a toxic effect, with the highest cumulative value being 0.94 μg/L (AT-3982) and copper toxicity in phytoplankton being reported at concentrations of 11 to 200 ppm (11,000-200,00 ug/L) (Mann et al. 2002). The relative impacts of other trace metals released by aerosols are not well understood, however ongoing research is being conducted to investigate their impacts in HNLC regions (Browning et al. 2018).

6. Conclusions

Our research demonstrates that easily reducible iron is three times greater in glacier-derived sediments than in desert-derived sediments, which supports the hypothesis that physically weathered dust contains more easily reducible iron than chemically weathered dust

per unit mass. This has implications for the outsized role that Alaskan dust may play in fertilizing phytoplankton in the northeastern subarctic Pacific. The solubility of these lithogenic aerosol sources also supports the hypothesis that Alaskan dust contributes more soluble iron per unit mass than Asian dust. In contrast, the volcanic ash unexpectedly had the lowest cumulative fractional iron solubility, consistent with low amounts of easily reducible and reducible iron. While Fe-bearing salts may be present in the volcanic ash, as evidenced by the moderate amounts of exchangeable Fe (II) measured, they do not appear to be abundant enough to drive high iron solubility. The low fractional iron solubility of the ash and low amounts of easily reducible Fe, while surprising, support previous research showing that iron speciation affects solubility in dust, with more reducible forms of iron being more soluble (Schroth et al. 2009). As climate change alters glacier mass balance, wind patterns, and dust transport, knowing the relative roles of these mineral dust and volcanic ash sources is important to understanding how these geologic changes impact carbon sequestration and food web dynamics.

Potential direction for future work

- Geochemical characterization of environmentally-aged ash in order to compare with fresh ash samples. *(In progress in the Koffman lab)*
- Constraining the relative fluxes of different aerosol sources to the northeastern subarctic Pacific.

7. Figures

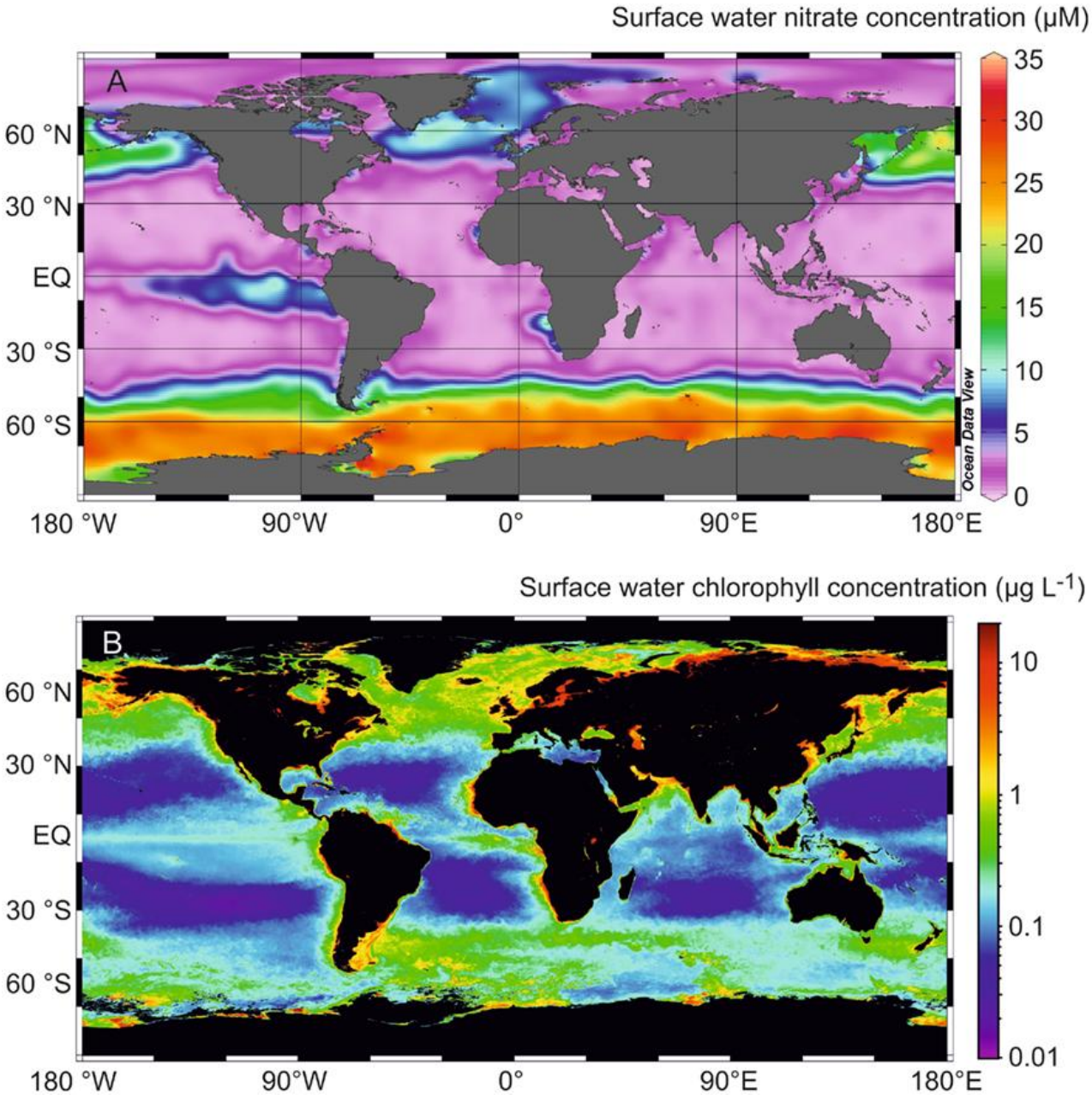

Figure 1. Global high nutrient (nitrate), low chlorophyll regions. Upper map shows nitrate concentration, lower map shows chlorophyll concentration. Our study region falls between ~35˚ N to ~ 62˚ N and ~135˚ W to ~180˚ W. Figure from Gledhill and Buck 2012.

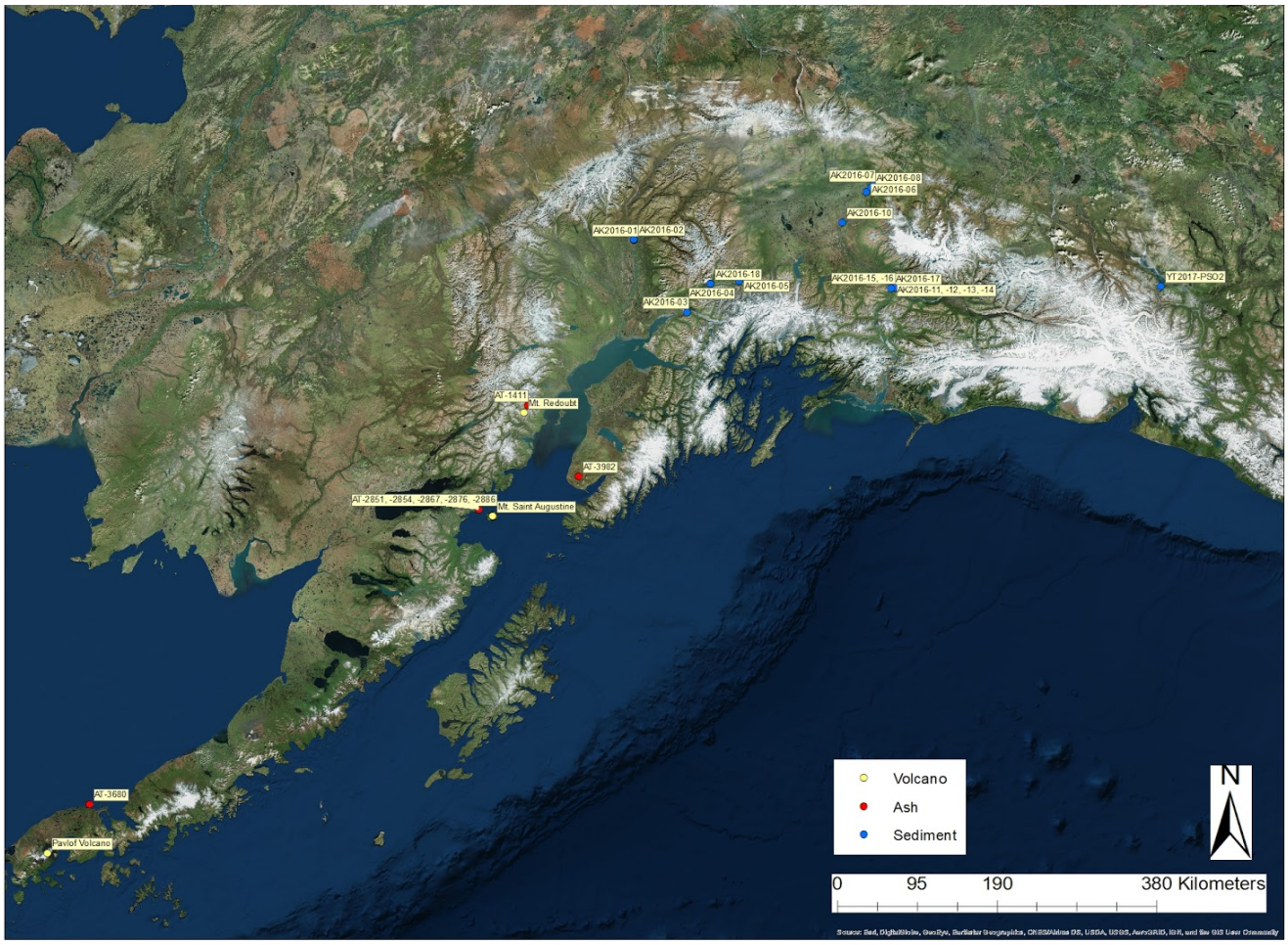

Figure 2. Map showing locations of sediment samples analyzed in this study and source volcanoes for ash samples. Drafted in ArcGIS by Zane Fields. GIS map sources: GeoEye, CNES/Alrius DS, USDA, USGS, AeroGRID, ISN, and the GIS User Community.

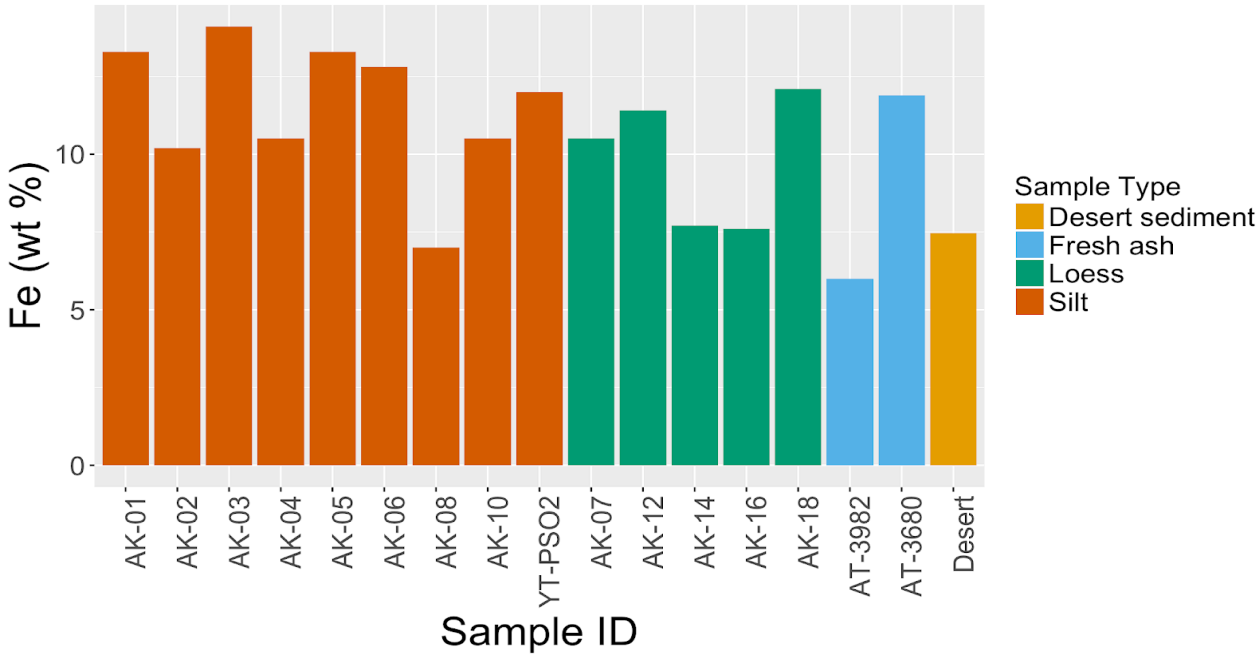

Figure 3. Total iron content of fresh ash and glacier-derived sediments, including both river silt and loess. "Desert sediment" is the average for desert-derived sediments from Lu et. al. 2017 (n = 108).

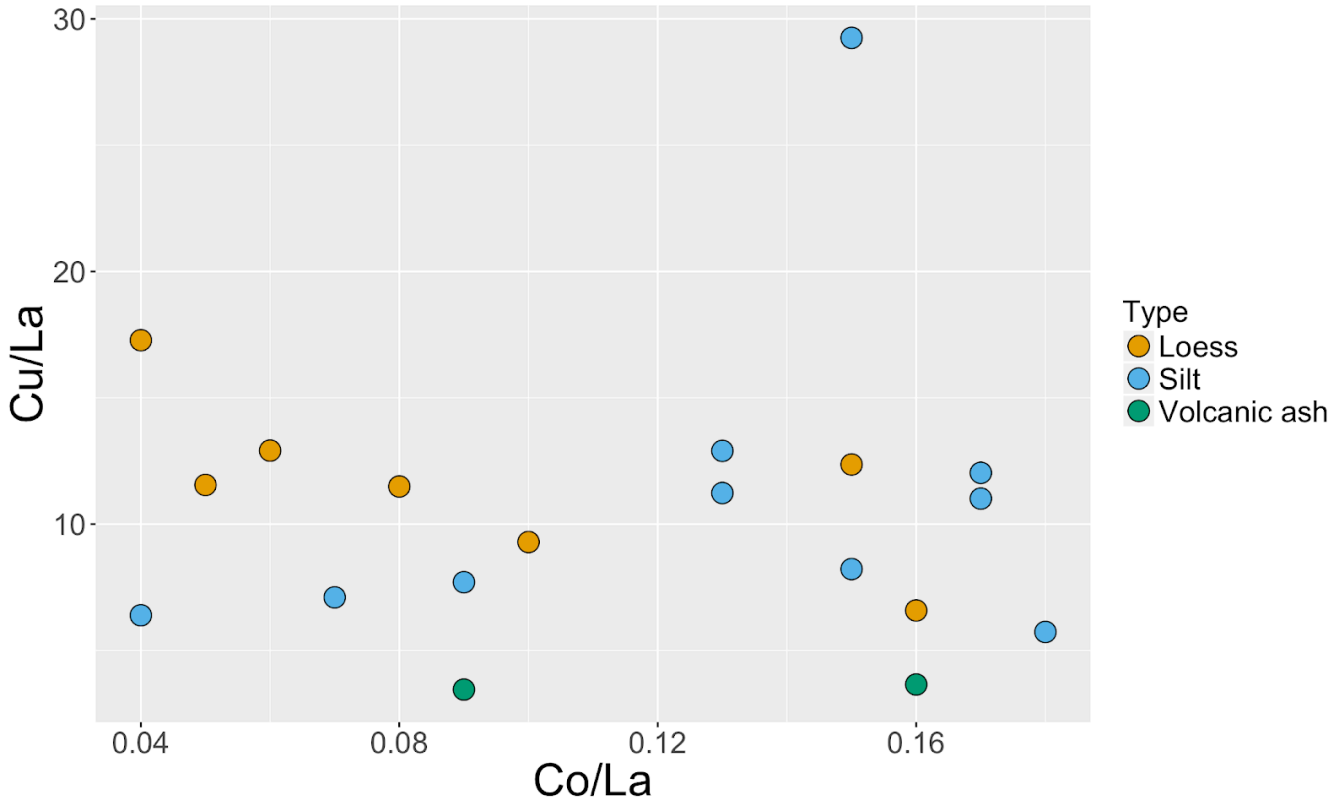

Figure 4. Ratios of copper and cobalt to lanthanum in completely digested <5 µm grain size fraction samples. Elements are standardized to lanthanum concentration to emphasize visual variability.

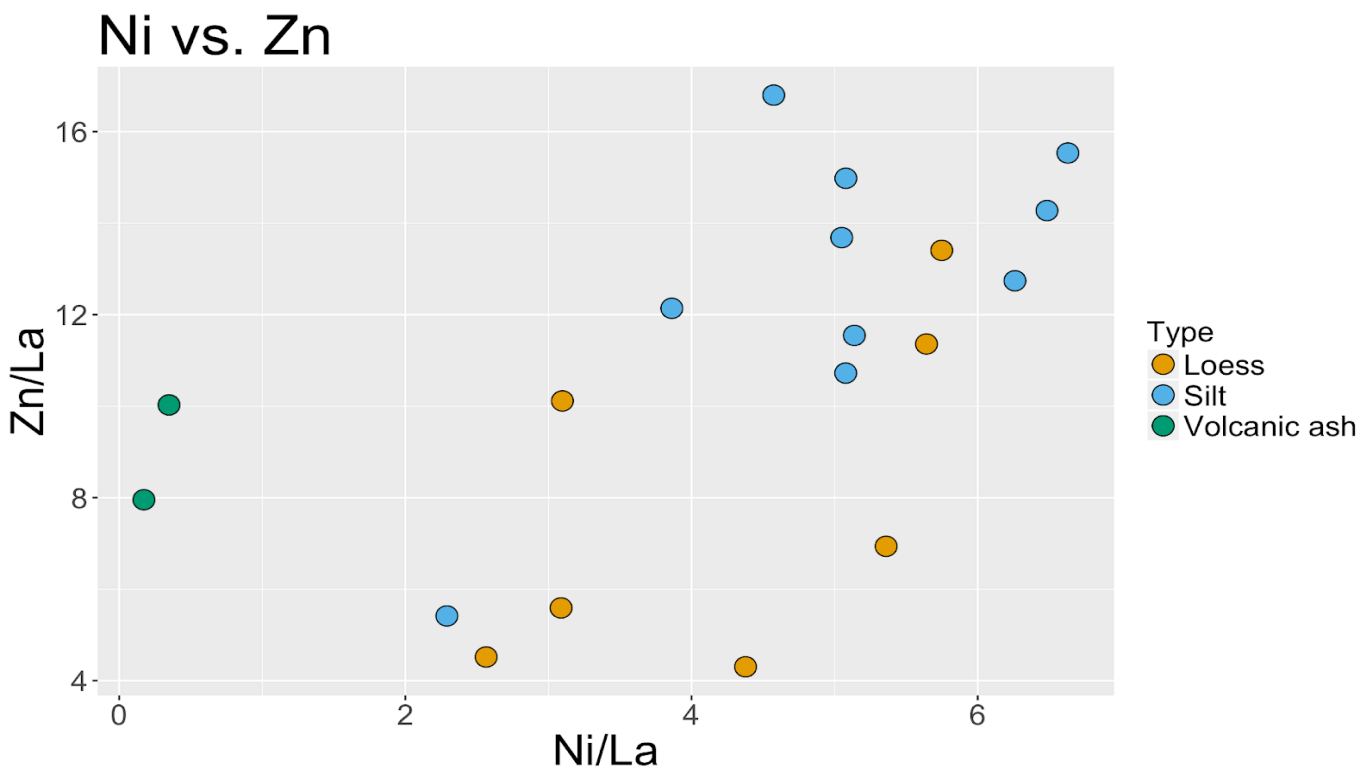

Figure 5. Ratios of zinc and nickel to lanthanum in completely digested <5 µm grain size fraction samples. Elements are standardized to lanthanum concentration to emphasize visual variability.

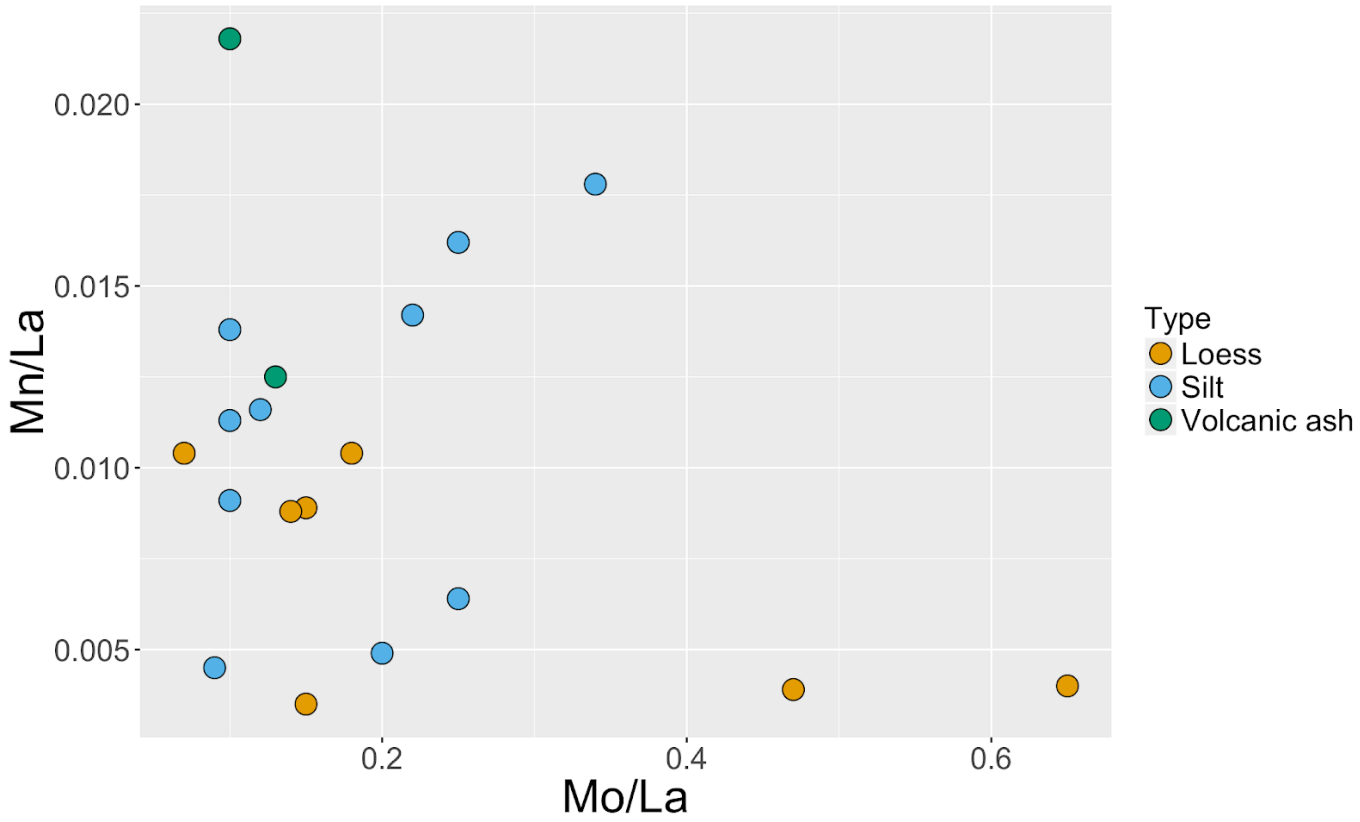

Figure 6. Concentration of manganese and molybdenum in completely digested <5 µm grain size fraction samples. Elements are standardized to lanthanum concentration to emphasize visual variability.

a.

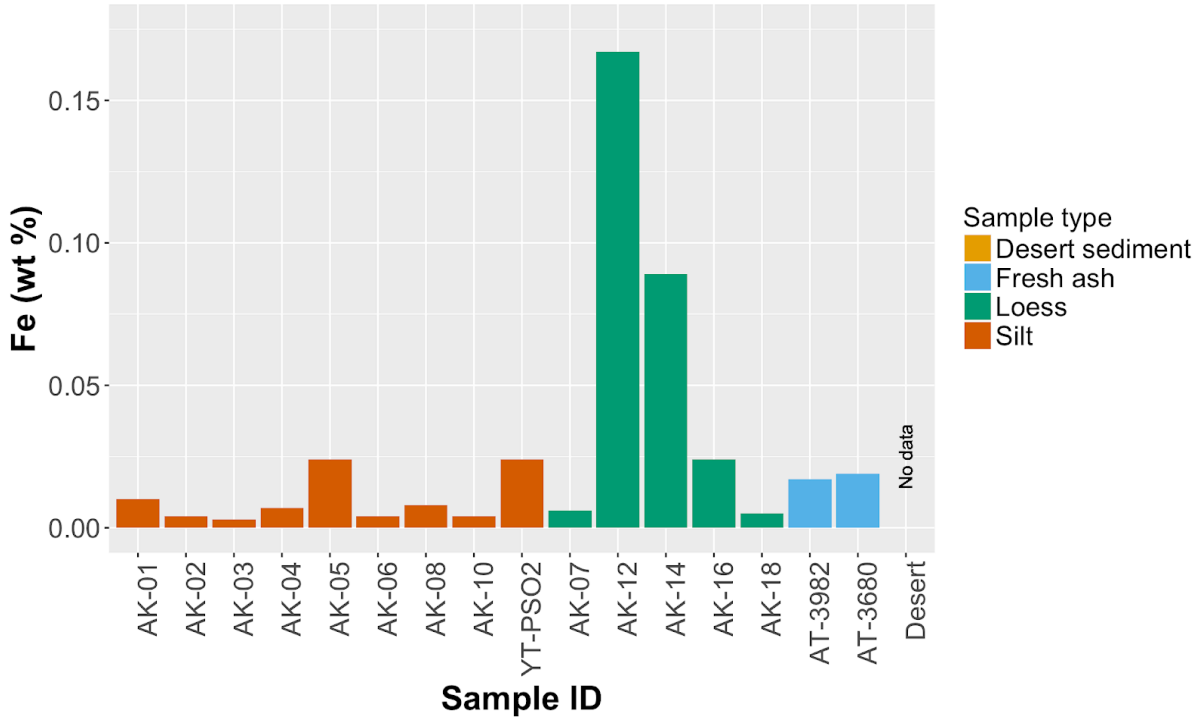

b

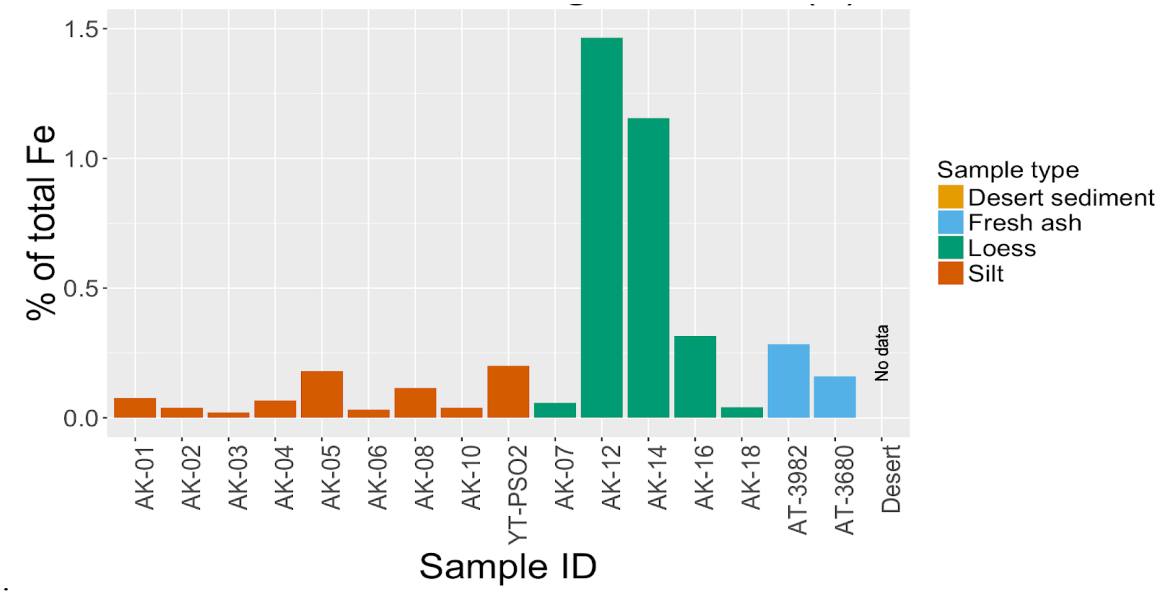

.

Figure 7. a) Iron in the form of exchangeable Fe (II) ions (extracted by magnesium chloride solution). **b)** Proportion of total iron in the form of exchangeable Fe (II) ions.

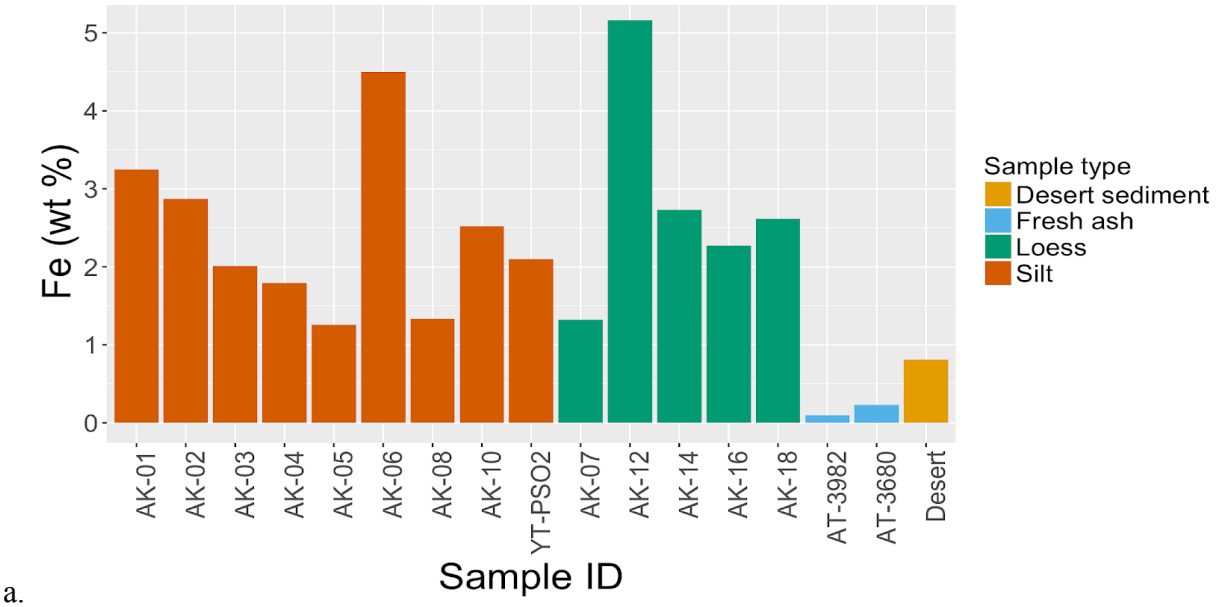

a.

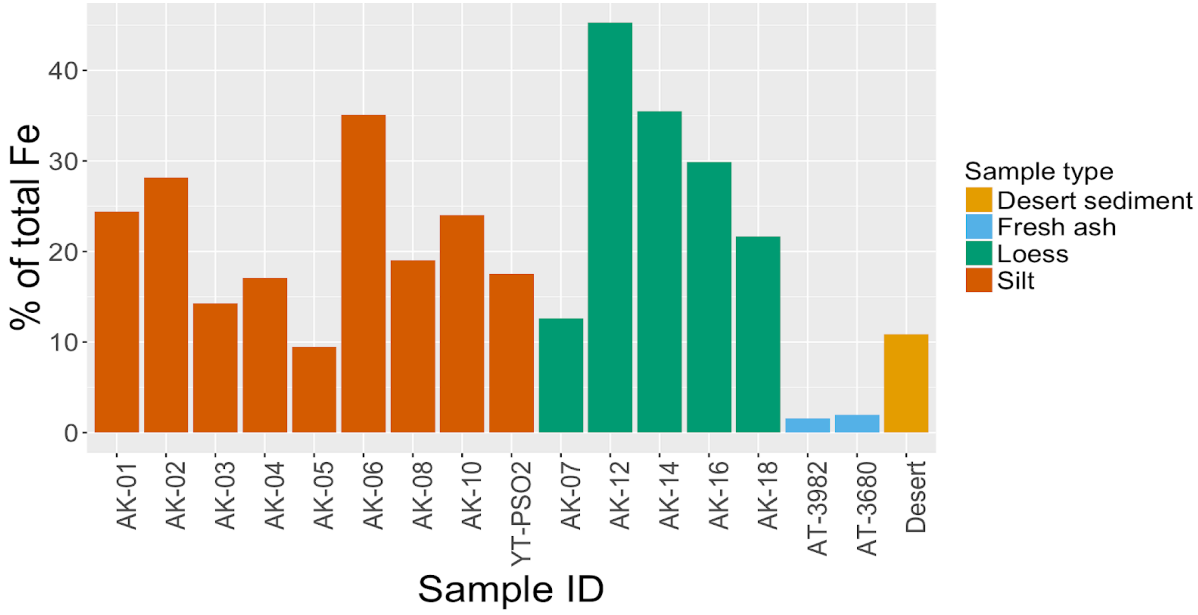

b.

Figure 8. a) Easily reducible iron content. **b)** Proportion of total iron that is easily reducible. "Desert sediment" is the average for desert-derived sediments from Lu et. al. 2017 (n = 108).

a.

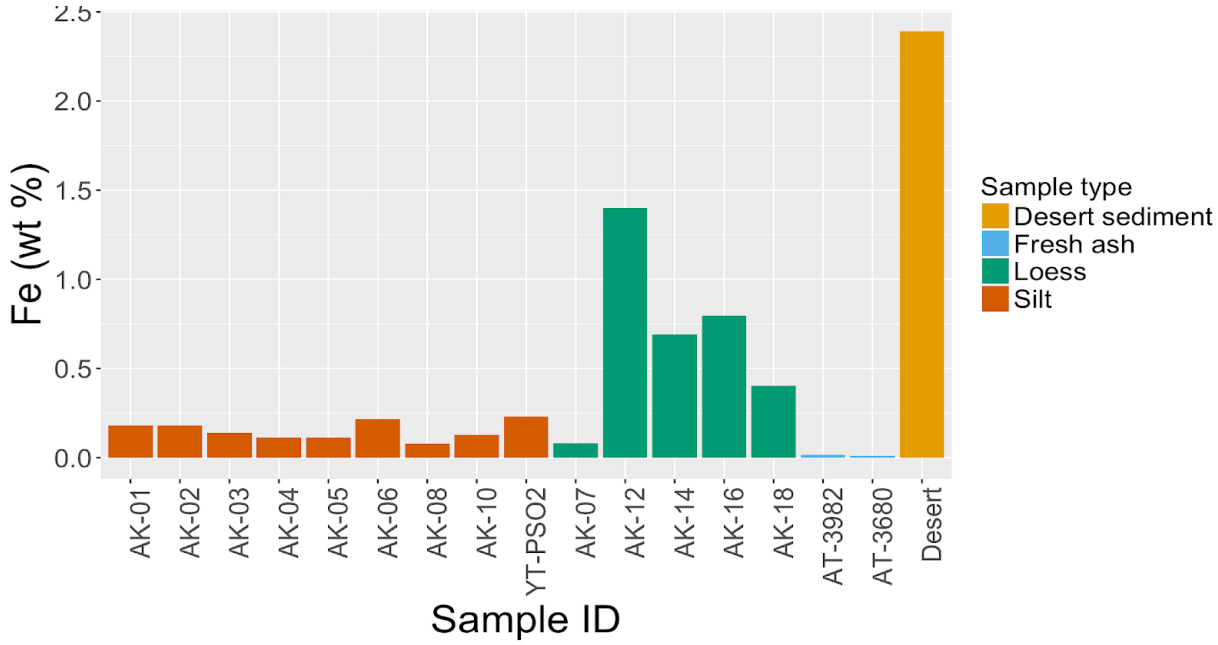

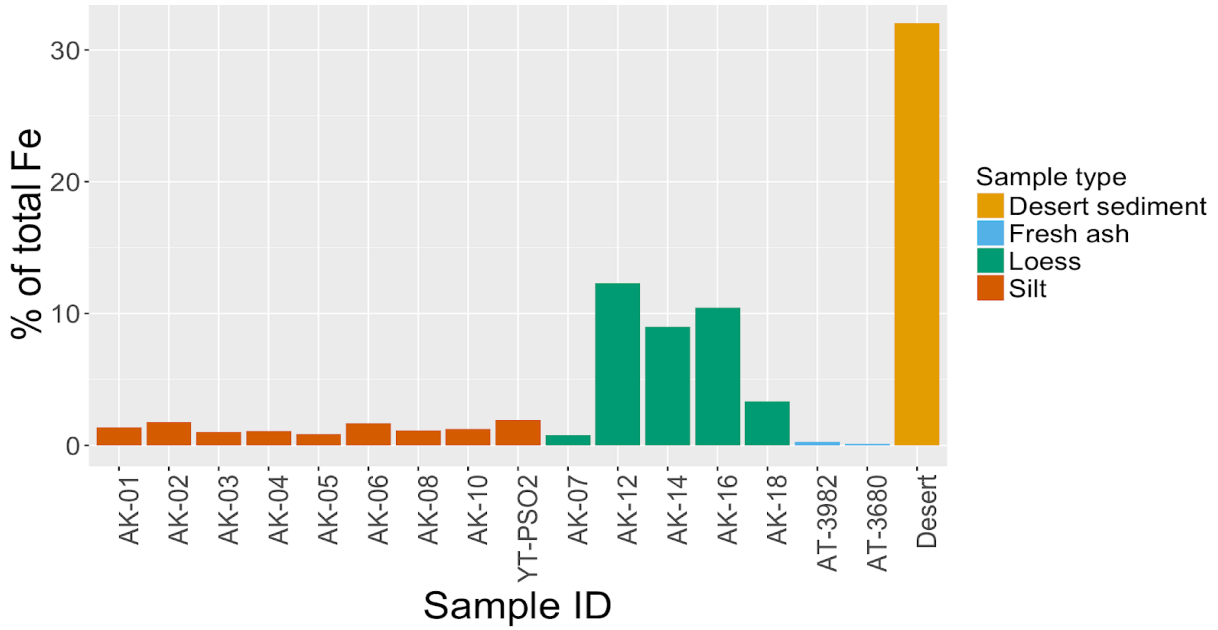

b.

Figure 9. a) Reducible iron content. b) Proportion of iron that is reducible. "Desert sediment" is the average for desert-derived sediments from Lu et. al. 2017 (n = 108).

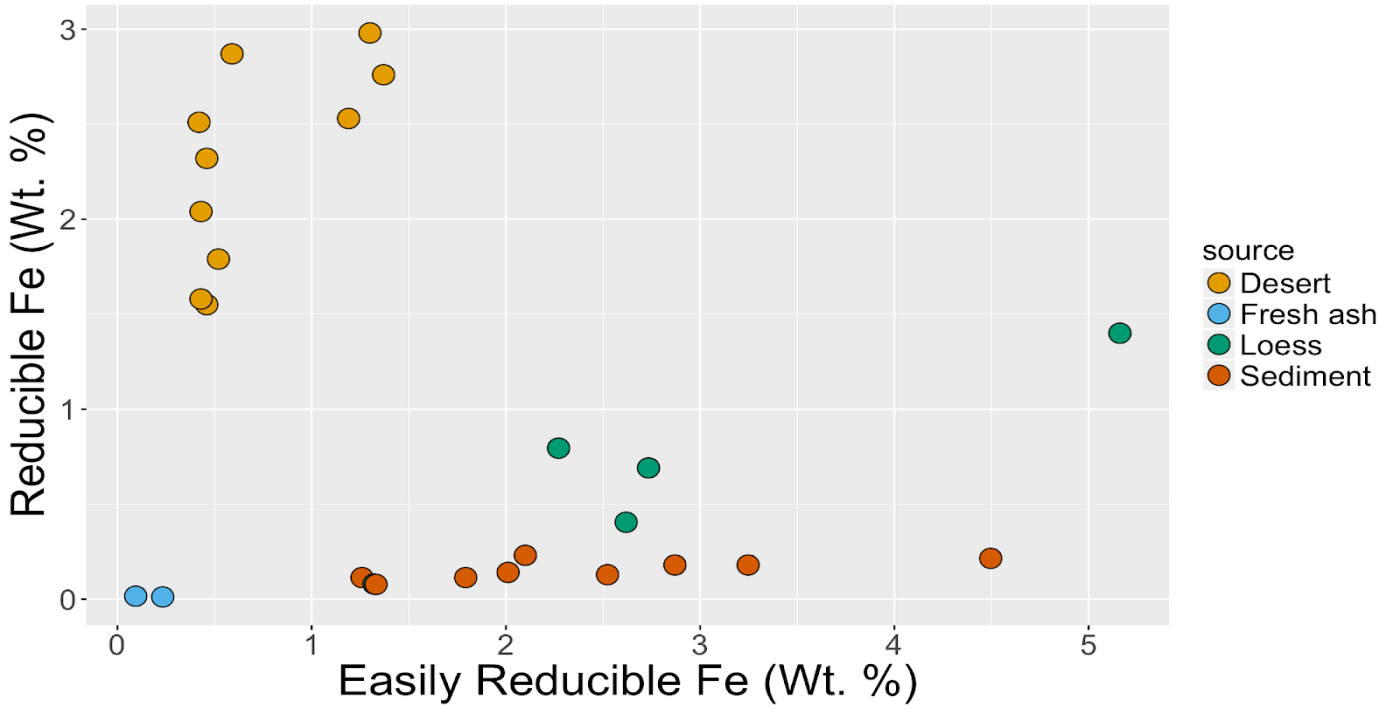

Figure 10. Proportions of total iron in the form of easily reducible iron and reducible iron. "Desert" samples are desert-derived sediments from Lu et. al. 2017, each dot represents the average from a given region.

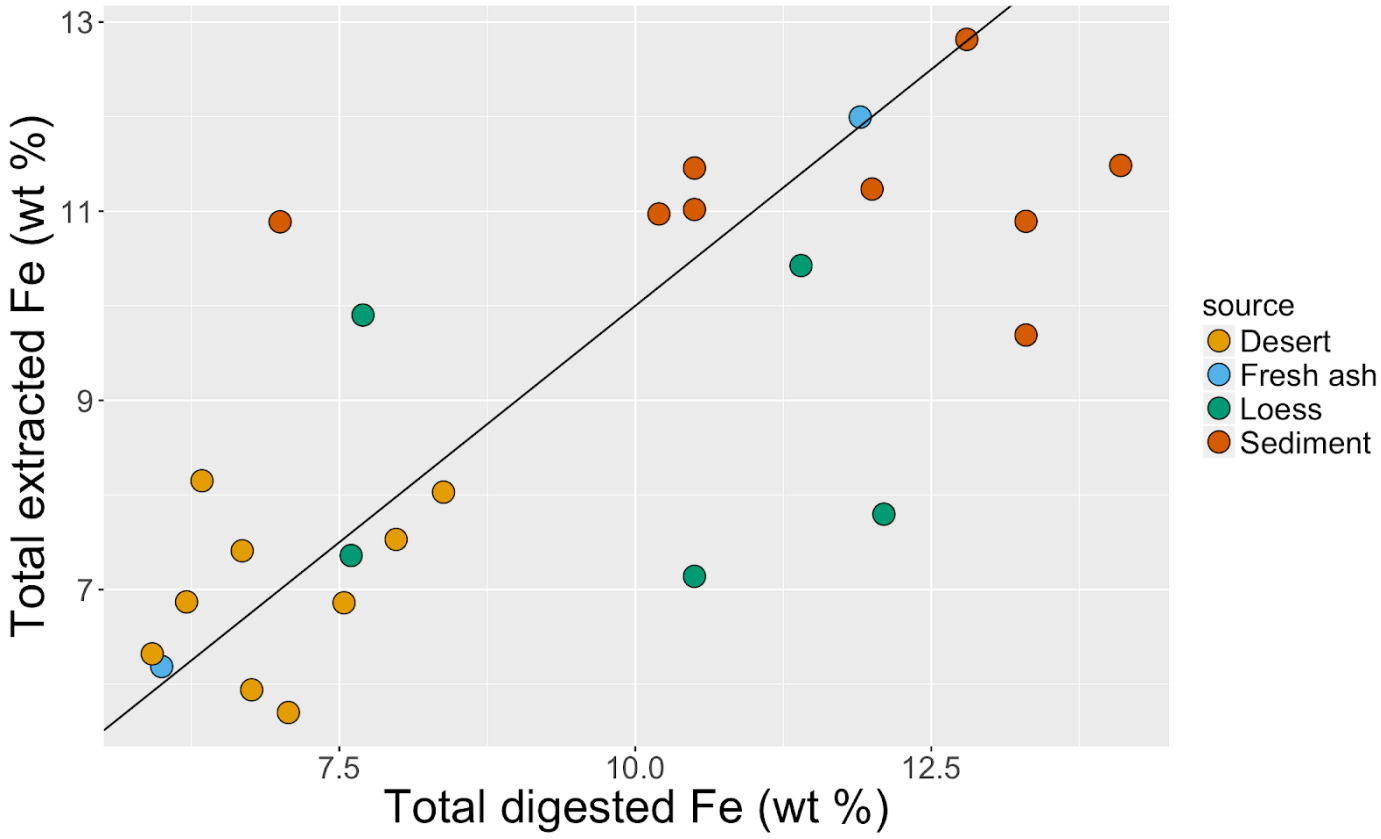

Figure 11. The total amount of iron determined by complete digestion compared to the sum of the iron from all the extraction steps. The desert samples are from Lu et. al 2017. Each dot represents the average from a particular desert (n=5-37). Total iron was determined by summing the data from the sequential extractions, found in Lu et al. supplemental materials. The line represents a 1:1 ratio.

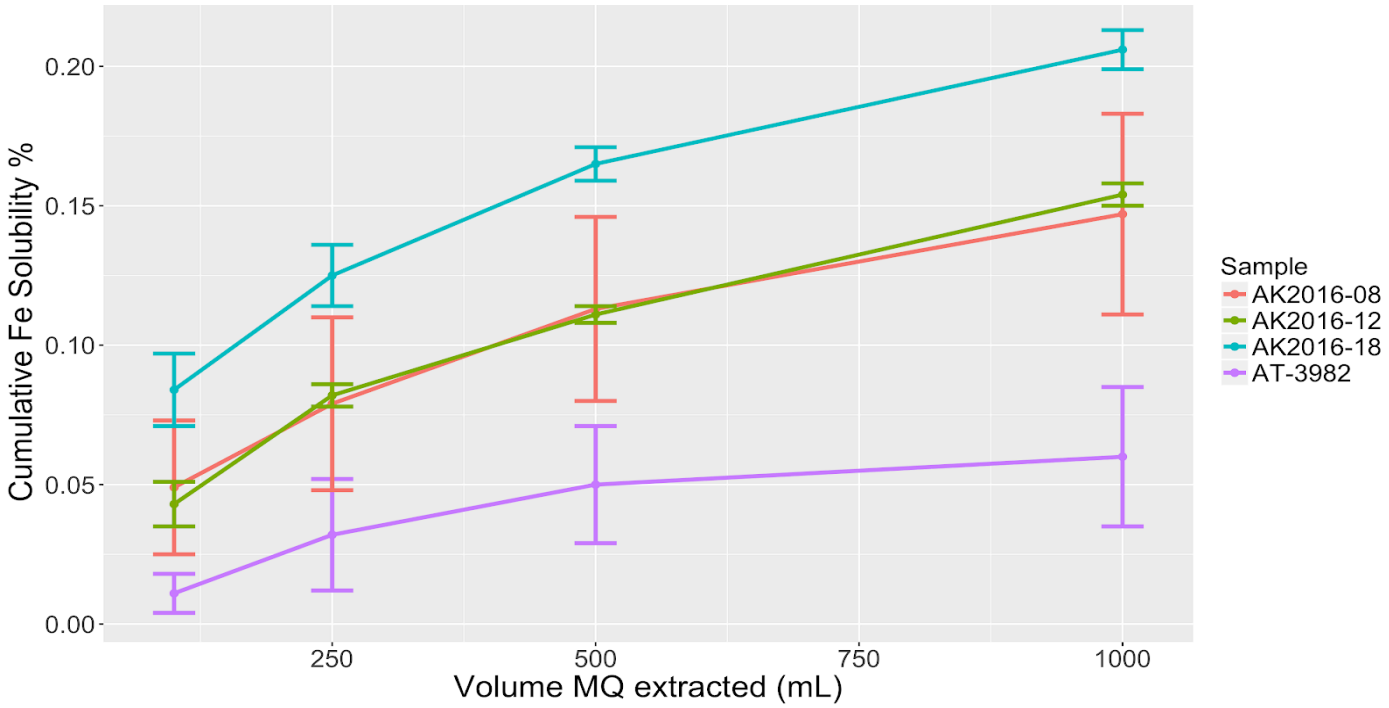

Figure 12. The cumulative fractional iron solubility for a total of 1000 mL of Milli-Q leaching.

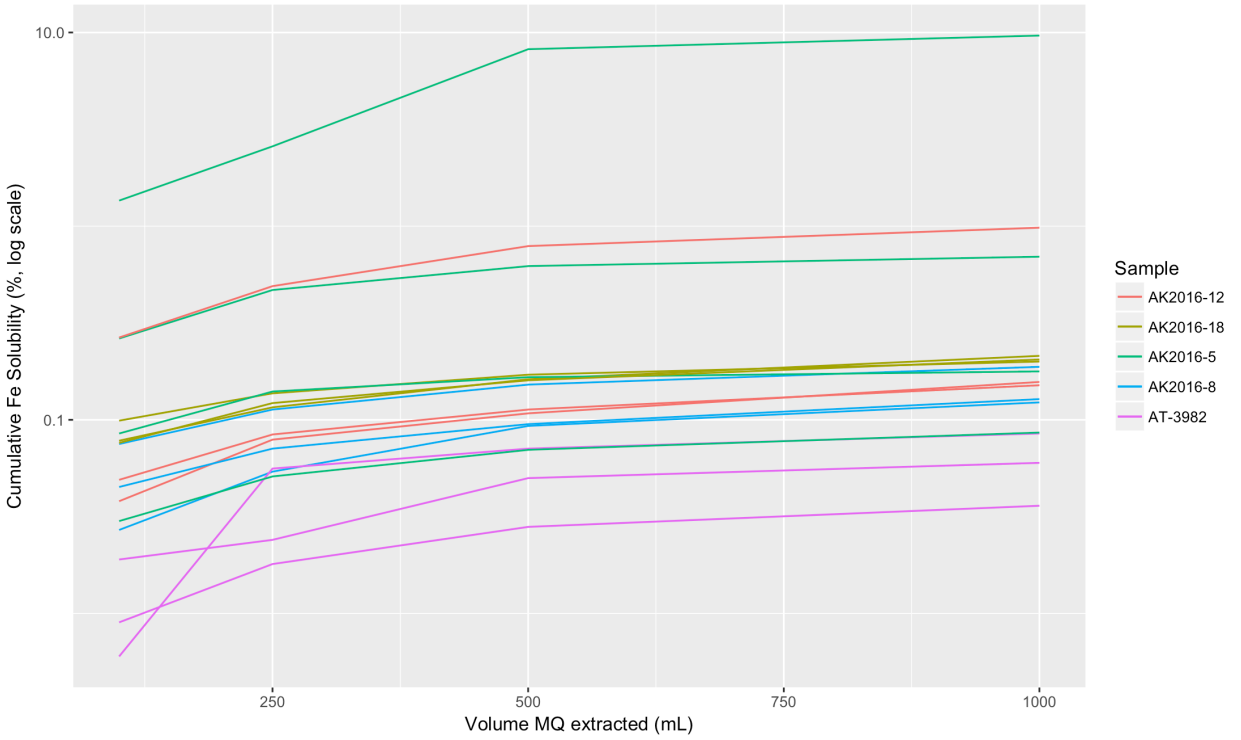

Figure 13. Cumulative iron solubility of replicates of Milli-Q leaches, log scale.

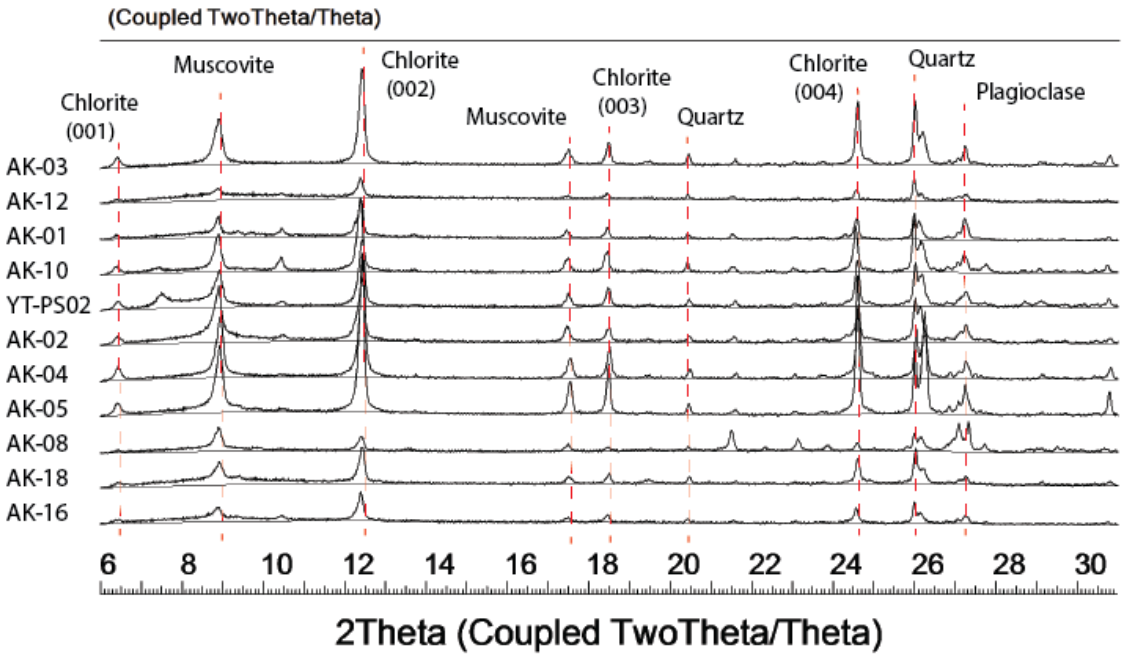

Figure 14. XRD spectra of <5 µm grain size fraction Alaskan glacial sediments. Spectra are offset from each other on the Y-axis by 2000 counts.

a.

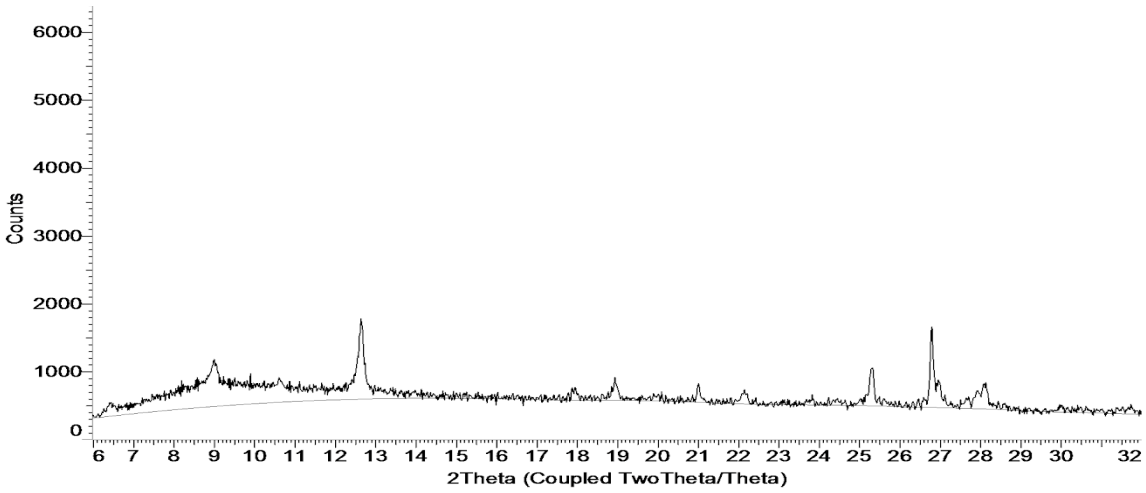

b.

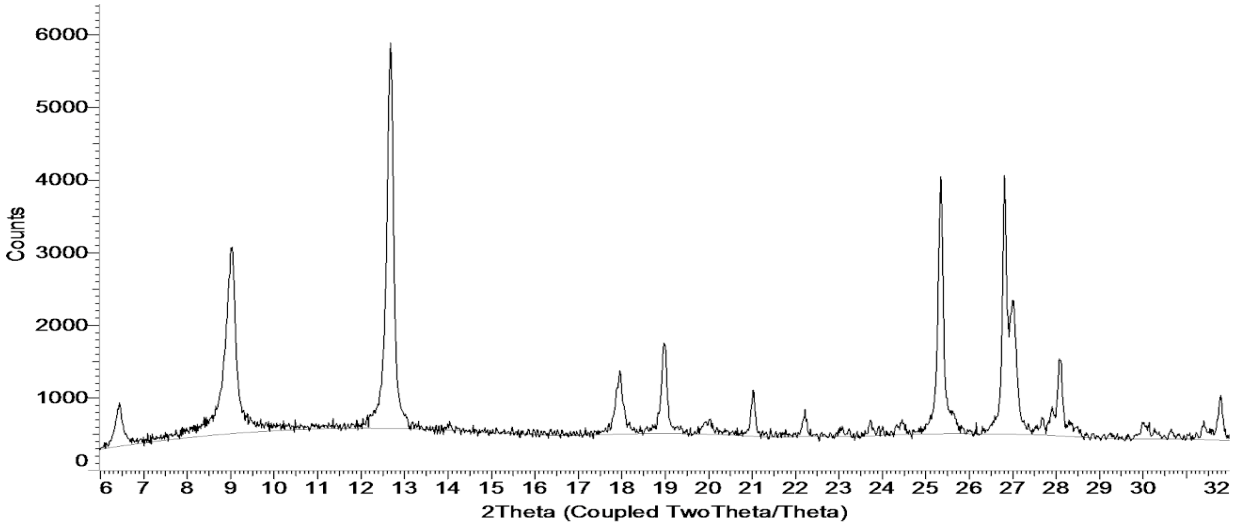

Figure 15 a. XRD spectra of AK2016-12, which has chlorite 002 and 004 peaks below 2000 counts and 2.65 wt % iron contained in oxyhydr(oxides) and sheet silicates. **b.** XRD spectra of AK2016-03, which has chlorite 002 and 004 peaks above 4000 counts and 8.228 wt % iron contained in oxyhydr(oxides) and sheet silicates.

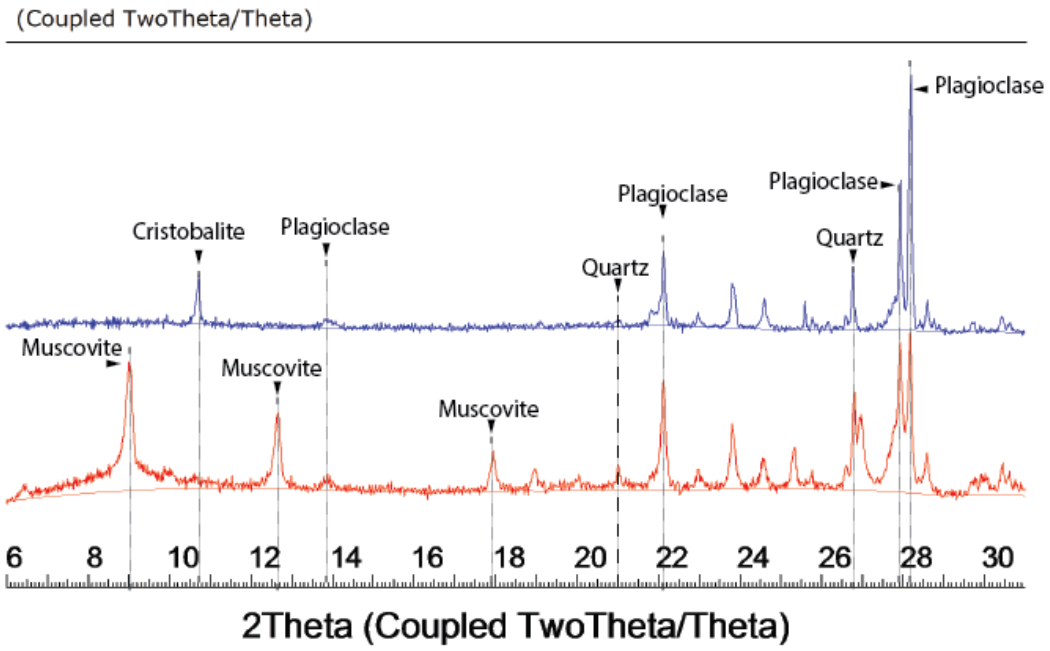

Figure 16. XRD spectra for bulk fresh ash samples. AT-3680 is from Mt. Pavlof and AT-3982 is from Mt. Redoubt. Spectra are offset from each other on the Y-axis by 1800 counts.

8. Tables

Table 1. Total iron and sequential iron extractions data.

Sample ID	Sample type	Total Fe (wt %)	Exchangeable Fe (II) (wt %)	Easily reducible Fe (wt %)	Reducible Fe (wt %)	Oxyhydr(oxides) and sheet silicate Fe (wt %)	Residual Fe (wt %)
AK2016-01	River silt	13.30	0.02	6.68	0.37	0.29	1.63
AK2016-02	River silt	10.20	0.01	5.91	0.37	0.31	1.56
AK2016-03	River silt	14.10	0.01	4.14	0.29	0.38	1.59
AK2016-04	River silt	10.50	0.01	3.69	0.23	0.37	1.98
AK2016-05	River silt	13.30	0.05	2.59	0.24	0.32	1.99
AK2016-06	River silt	12.80	0.01	9.25	0.44	0.30	2.35
AK2016-07	Loess	10.50	0.01	2.72	0.16	0.36	1.65
AK2016-08	River silt	7.00	0.02	2.74	0.16	0.17	2.75
AK2016-10	River silt	10.50	0.01	5.19	0.27	0.30	2.45
AK2016-11	Loess	9.68					
AK2016-12	Loess	11.40	0.34	10.62	2.88	0.12	0.76
AK2016-13	Loess	7.58					
AK2016-14	Loess	7.70	0.18	5.63	1.42	0.14	1.15
AK2016-16	Loess	7.60	0.05	4.67	1.64	0.19	0.89
AK2016-17	River silt	9.84					
AK2016-18	Loess	12.10	0.01	5.39	0.83	0.33	1.56
YT2017-PS02	River silt	12.00	0.05	4.32	0.47	0.35	1.46
AT-3982	Fresh ash	6.00	0.04	0.19	0.03	0.14	4.29
AT-3680	Fresh ash	11.90	0.04	0.48	0.03	0.11	13.63

Table 2. Comparison of iron content of glacial and desert sediments. Desert values from Lu et al. 2017.

	Glacial sediment samples (n=17)	**Desert sediment samples (n=62-125)**
Minimum total iron content measured (wt %)	7.00	5.92
Maximum total iron content measured (wt %)	14.10	8.38
Mean total iron content (wt %)	10.9	7.46
Easily reducible iron	2.55	0.81
Reducible iron	0.34	2.39
Iron in oxyhydr(oxides) and sheet silicates	6.13	3.15
Residual iron	1.17	0.88

Table 3. Major elements.

Sample	Type	Na (wt %)	Mg (wt %)	Al (wt %)	P (wt %)	K (wt %)	Ca (wt %)	Mn (wt %)	Ti (wt %)
AK2016-01	Silt	6.4	4.3	25.11	0.42	3.26	5.3	0.31	0.9
AK2016-02	Silt	4.5	3.4	20.93	0.42	3.26	3.34	0.21	0.76
AK2016-03	Silt	4.82	5.02	26.78	0.46	6.94	2.31	0.28	1.18
AK2016-04	Silt	4.14	4.29	21.41	0.3	4.32	3.07	0.16	0.83
AK2016-05	Silt	4.72	5.5	25.18	0.27	4.96	3.99	0.24	1.02
AK2016-06	Silt	3.9	4.61	20.13	0.41	3.76	4.97	0.13	0.9
AK2016-07	Loess	3.77	4.46	19.64	0.22	2.62	5.11	0.14	0.91
AK2016-08	Silt	4.7	3.16	19.2	0.45	2.87	5.23	0.09	0.84
AK2016-10	Silt	2.99	5.01	19.4	0.4	3.17	5.23	0.17	0.87
AK2016-11	Loess	3.81	2.71	14.02	0.68	1.7	3.24	0.07	0.65
AK2016-12	Loess	4.8	2.1	12.3	0.7	1.3	5	0.1	0.6
AK2016-13	Loess	3.96	1.97	10.76	0.89	1.11	5.29	0.11	0.37
AK2016-14	Loess	4.67	2.25	12.63	0.77	1.23	4	0.06	0.54
AK2016-16	Loess	4.05	2.51	12.17	0.73	1.35	5.19	0.17	0.49
AK2016-17	Silt	3.71	4.44	19.46	0.38	2.85	5.2	0.18	0.82
AK2016-18	Loess	3.96	3.21	20.93	0.5	3.44	2.68	0.17	0.68
YT2017-PS02	Silt	4.68	5.64	20.33	0.38	4.35	5.04	0.11	0.82
AT-3982	Volcanic ash	6.12	2.66	20.89	0.24	2.04	4.94	0.14	0.5
AT-3680	Volcanic ash	8.04	5.34	23.87	0.46	1.32	5.02	0.24	1.4

Table 4. Trace elements

Sample	Type	Cr (ppm)	Co (ppm)	Ni (ppm)	Cu (ppm)	Zn (ppm)	Mo (ppm)	Cd (ppm)	La (ppm)
AK2016-01	Silt	104.5	2.33	67.2	224.4	211.2	6.0	0.1	17.4
AK2016-02	Silt	85.0	2.22	67.7	432.9	248.6	3.2	0.2	14.8
AK2016-03	Silt	231.2	2.89	114.7	208.1	268.7	4.3	0.2	17.3
AK2016-04	Silt	103.0	2.38	71.7	156.3	194.3	1.4	0.1	14.2
AK2016-05	Silt	134.7	3.18	89.4	99.7	200.9	1.7	0.1	17.4
AK2016-06	Silt	146.1	1.86	103.6	157.1	305.6	5.1	0.6	20.4
AK2016-07	Loess	90.4	2.02	75.6	165.6	152.2	1.0	0.2	13.4
AK2016-08	Silt	53.4	0.87	45.8	127.7	108.3	1.8	0.1	20
AK2016-10	Silt	139.2	2.37	120.6	208.8	265.5	1.8	0.6	18.6
AK2016-11	Loess	129.4	1.06	93.8	226.0	121.4	11.4	0.1	17.5
AK2016-12	Loess	151.2	1.04	112.5	444.0	110.6	12.1	0.2	25.7
AK2016-13	Loess	51.1	1.18	38.1	114.3	124.4	1.9	0.1	12.3
AK2016-14	Loess	64.2	0.84	43.6	196.4	76.8	2.5	0.1	17
AK2016-16	Loess	64.3	1.59	59.6	221.7	107.9	2.7	0.2	19.3
AK2016-17	Silt	85.2	2.25	78.7	127.4	166.2	1.9	0.2	15.5
AK2016-18	Loess	107.1	2.60	93.7	107.2	218.5	3.0	0.2	16.3
YT2017-PS02	Silt	169.1	1.52	139.6	158.3	284.1	4.4	0.3	22.3
AT-3982	Volcanic ash	9.6	1.77	3.9	40.9	112.3	1.4	0.1	11.2
AT-3680	Volcanic ash	1.7	1.02	1.9	37.9	87.5	1.1	0.1	11

9. References

Aguilar-Islas, A.M., Wu, J., Rember, R., Johansen, A.M., and Shank, L.M., 2010, Dissolution of aerosol-derived iron in seawater: Leach solution chemistry , aerosol type , and colloidal iron fraction: Marine Chemistry, v. 120, p. 25–33, doi: 10.1016/j.marchem.2009.01.011.

Andreae, M.O., 2007, Aerosols before pollution: Science, v. 315, p. 50–51, doi: 10.1126/science.1136529.

Arking, A., 1991, The Radiative Effects of Clouds and their Impact on Climate: Bulletin American Meteorological Society, v. 72, p. 795–814.

Aumont, O., and Bopp, L., 2006, Globalizing results from ocean in situ iron fertilization studies: Global Biogeochemical Cycles, v. 20, p. 1–15, doi: 10.1029/2005GB002591.

Baeyens, W., Bowie, A.R., Buesseler, K., Elskens, M., Gao, Y., Lamborg, C., Leermakers, M., Remenyi, T., and Zhang, H., 2011, Size-fractionated labile trace elements in the Northwest Pacific and Southern Oceans: Marine Chemistry, v. 126, p. 108–113, doi: 10.1016/j.marchem.2011.04.004.

Baker, A.R., and Croot, P.L., 2010, Atmospheric and marine controls on aerosol iron solubility in seawater: Marine Chemistry, v. 120, p. 4–13, doi: 10.1016/j.marchem.2008.09.003.

Bishop, J.K.B., Davis, R.E., Sherman, J.T., Division, E.S., and Berkeley, L., 2000, Robotic Observations of Dust Storm Enhancement of Carbon Biomass in the North Pacific: Science, v. 298, p. 817–822.

Boyd, P.W., Jickells, T., Law, C.S., Blain, S., Boyle, E.A., Buesseler, K.O., Coale, K.H., Cullen, J.J., Baar, H.J.W. De, Follows, M., Harvey, M., Lancelot, C., and Levasseur, M., 2007, Mesoscale Iron Enrichment Experiments 1993–2005: Synthesis and Future Directions: Science, v. 315, p. 612–617.

Banner, J.L., 2004, Radiogenic isotopes: Systematics and applications to earth surface processes and chemical stratigraphy: Earth-Science Reviews, v. 65, p. 141–194, doi: 10.1016/S0012-8252(03)00086-2.

Benner, R., 2011, Loose ligands and available iron in the ocean: Proceedings of the National Academy of Sciences, v. 108, p. 893–894, doi: 10.1073/pnas.1018163108.

Browning, T.J., Bouman, H.A., Henderson, G.M., Mather, T.A., Pyle, D.M., Schlosser, C., Woodward, E.M.S., and Moore, C.M., 2014, Strong responses of Southern Ocean phytoplankton communities to volcanic ash: Geophysical Research Letters, v. 41, p. 2851–2857, doi: 10.1002/2014GL059364.Received.

Browning, T.J., Stone, K., Bouman, H.A., Mather, T.A., Pyle, D.M., Moore, C.M., and Martinez-Vicente, V., 2015, Volcanic ash supply to the surface ocean- remote sensing of biological responses and their wider biogeochemical significance: Frontiers in Marine Science, v. 2, p. 1–22, doi: 10.3389/fmars.2015.00014.

Browning, T.J., Rapp, I., Schlosser, C., Gledhill, M., Achterberg, E.P., Bracher, A., and Le Moigne, F.A.C., 2018, Influence of Iron, Cobalt, and Vitamin B12 Supply on Phytoplankton Growth in the Tropical East Pacific During the 2015 El Niño: Geophysical Research Letters, v. 45, p. 6150–6159, doi: 10.1029/2018GL077972.

Capitani, G., Miyajima, N., Sulpizio, R., D'Addabbo, M., Galimberti, L., Guidi, M., and Andreozzi, G.B., 2018, Iron release in aqueous environment by fresh volcanic ash from Mount Etna (Italy) and Popocatépetl (Mexico) volcanoes: Environmental Earth Sciences, v. 77, doi: 10.1007/s12665-018-7692-z.

Chester, R., and Hughes, M.J., 1967, A Chemical Technique for the Separation of Ferro-Manganese Minerals, Carbonate Minerals, and Adsorbed Trace Elements from Pelagic Sediments: Chemical Geology, v. 2, p. 249–262.

Crusius, J., Schroth, A.W., Gassó, S., Moy, C.M., Levy, R.C., and Gatica, M., 2011, Glacial flour dust storms in the Gulf of Alaska: Hydrologic and meteorological controls and their importance as a source of bioavailable iron: Geophysical Research Letters, v. 38, p. n/a-n/a, doi: 10.1029/2010GL046573.

De La Rocha, C.L. and Passow, U., 2007, Factors influencing the sinking of POC and the efficiency of the biological carbon pump: Deep Sea Research Part II: Topical Studies in Oceanography, v. 54, p. 639-658.

Ding, Z.L., Yang, S.L., Sun, J.M., and Liu, T.S., 2001, Iron geochemistry of loess and red clay deposits in the Chinese Loess Plateau and implications for long-term Asian monsoon evolution in the last 7.0 Ma: Earth and Planetary Science Letters, v. 185, p. 99–109, doi: 10.1016/S0012-821X(00)00366-6.

Dubischar, C.D., and Bathmann, U. V., 1997, Grazing impact of copepods and salps on phytoplankton in the Atlantic sector of the Southern Ocean: Deep-Sea Research Part II: Topical Studies in Oceanography, v. 44, p. 415–433.

Ducklow, H.W., Steinberg, D.K., and Buesseler, K.O., 2001, Upper Ocean Carbon Export and the Biological Pump: v. 14, p. 56008–56016.

Edwards, A.M., Platt, T., and Sathyendranath, S., 2004, The high-nutrient, low-chlorophyll regime of the ocean: Limits on biomass and nitrate before and after iron enrichment: Ecological Modelling, v. 171, p. 103–125, doi: 10.1016/j.ecolmodel.2003.06.001.

Farmer, D.K., Cappa, C.D., and Kreidenweis, S.M., 2015, Atmospheric Processes and Their Controlling Influence on Cloud Condensation Nuclei Activity: Chemical Reviews, v. 115, p. 4199–4217, doi: 10.1021/cr5006292.

Field, C.B., Behrenfeld, M.J., and Randerson, J.T., 1998, Primary Production of the Biosphere : Integrating Terrestrial and Oceanic Components: Science, v. 281, p. 237–240, doi: 10.1126/science.281.5374.237.

Flower, V.J.B., and Kahn, R.A., 2017a, Distinguishing Remobilized Ash From Erupted Volcanic Plumes Using Space-Borne Multiangle Imaging: Geophysical Research Letters, v. 44, p. 10,772-10,779, doi: 10.1002/2017GL074740.

Flower, V.J.B., and Kahn, R.A., 2017b, Assessing the altitude and dispersion of volcanic plumes using MISR multi-angle imaging from space: Sixteen years of volcanic activity in the

Kamchatka Peninsula, Russia: Journal of Volcanology and Geothermal Research, v. 337, p. 1–15, doi: 10.1016/j.jvolgeores.2017.03.010.

Frogner, P., Gíslason, S.R., and Óskarsson, N., 2001, Fertilizing potential of volcanic ash in ocean surface water: Geology, v. 29, p. 487–490, doi: 10.1130/0091-7613(2001)029<0487:FPOVAI>2.0.CO;2.

Giordano, M., Beardall, J., and Raven, J.A., 2005, CO2 Concentrating Mechanisms in Algae: Mechanisms, Environmental Modulation, and Evolution: Annual Review of Plant Biology, v. 56, p. 99–131, doi: 10.1146/annurev.arplant.56.032604.144052.

Gislason, S.R., Oelkers, E.H., Eiriksdottir, E.S., Kardjilov, M.I., Gisladottir, G., Sigfusson, B., Snorrason, A., Elefsen, S., Hardardottir, J., Torssander, P., and Oskarsson, N., 2009, Direct evidence of the feedback between climate and weathering: Earth and Planetary Science Letters, v. 277, p. 213–222, doi: 10.1016/j.epsl.2008.10.018.

Gledhill, M., and Buck, K.N., 2012, The organic complexation of iron in the marine environment: A review: Frontiers in Microbiology, v. 3, p. 1–17, doi: 10.3389/fmicb.2012.00069.

Global Volcanism Program, 2013. Volcanoes of the World, v. 4.7.4. Venzke, E (ed.). Smithsonian Institution. Downloaded 19 Nov 2018. https://doi.org/10.5479/si.GVP.VOTW4-2013

Green, A.R., DeBari, S.M., Kelemen, P.B., Blusztajn, J., and Clift, P.D., 2006, A detailed geochemical study of island Arc crust: The Talkeetna Arc section, south-central Alaska: Journal of Petrology, v. 47, p. 1051–1093, doi: 10.1093/petrology/egl002.

Grousset, F.E., and Biscaye, P.E., 2005, Tracing dust sources and transport patterns using Sr, Nd and Pb isotopes: Chemical Geology, v. 222, p. 149–167, doi: 10.1016/j.chemgeo.2005.05.006.

Goudie, A.S., and Middleton, N.J., 2001, Saharan dust storms: Nature and consequences: Earth-Science Reviews, v. 56, p. 179–204, doi: 10.1016/S0012-8252(01)00067-8.

Guan, Q., Sun, X., Yang, J., Pan, B., Zhao, S., and Wang, L., 2017, Dust Storms in Northern China: Long-Term Spatiotemporal Characteristics and Climate Controls: American Meteorological Society, v. 30, p. 6683–6700, doi: 10.1175/JCLI-D-16-0795.1.

Guo, Z., Liu, T., Fedoroff, N., Wei, L., Ding, Z., Wu, N., Lu, H., Jiang, W., and An, Z., 1998, Climate extremes in Loess of China coupled with the strength of deep-water formation in the North Atlantic: Global and Planetary Change, v. 18, p. 113–128, doi: 10.1016/S0921-8181(98)00010-1.

Guyon, P., Frank, G.P., Welling, M., Chand, D., Artaxo, P., Rizzo, L., Nishioka, G., Kolle, O., Fritsch, H., Silva Dias, M.A.F., Gatti, L. V., Cordova, A.M., and Andreae, M.O., 2005, Airborne measurements of trace gas and aerosol particle emissions from biomass burning in Amazonia: Atmospheric Chemistry and Physics, v. 5, p. 2989–3002, doi: 10.5194/acp-5-2989-2005.

Hamme, R.C., Webley, P.W., Crawford, W.R., Whitney, F.A., Degrandpre, M.D., Emerson, S.R., Eriksen, C.C., Giesbrecht, K.E., Gower, J.F.R., Kavanaugh, M.T., Peña, M.A., Sabine, C.L., Batten, S.D., Coogan, L.A., et al., 2010, Volcanic ash fuels anomalous plankton bloom in subarctic northeast Pacific: Geophysical Research Letters, v. 37, p. 1–5, doi: 10.1029/2010GL044629.

Heron, G., Crouzet, C., Bourg, A.C.M., and Christensen, T.H., 1994, Speciation of Fe(II) and Fe(III) in Contaminated Aquifer Sediments Using Chemical Extraction Techniques: Environmental Science and Technology, v. 28, p. 1698–1705, doi: 10.1021/es00058a023.

Hutchins, D.A., Witter, A.E., Butler, A., and Luther, G.W., 1999, Competition among marine phytoplankton for different chelated iron species: Nature, v. 400, p. 858–861, doi: 10.1038/23680.

Hyer, E.J., and Chew, B.N., 2010, Aerosol transport model evaluation of an extreme smoke episode in Southeast Asia: Atmospheric Environment, v. 44, p. 1422–1427, doi: 10.1016/j.atmosenv.2010.01.043.

Ito, A., and Shi, Z., 2015, Delivery of anthropogenic bioavailable iron from mineral dust and combustion aerosols to the ocean: Atmospheric Chemistry and Physics Discussions, v. 16, p. 85–99, doi: 10.5194/acpd-15-23051-2015.

Jickells, T.D., An, Z.S., Andersen, K.K., Baker, A.R., Bergametti, G., Brooks, N., Cao, J.J., Boyd, P.W., Duce, R.A., Hunter, K.A., Kawahata, H., Kubilay, N., LaRoche, J., Liss, P.S., et al., 2005, Global Iron Connections Between Desert Dust, Ocean Biogeochemistry, and Climate: Science, v. 308, p. 67–71, doi: 10.1126/science.1105959.

Koffman, B.G., Goldstein, S.L., Recasens, C., Kaplan, M.R., Borunda, A., and Winckler, G., 2018, Grain size effects on Sr-Nd-Pb isotopes in sediments and implications for provenance and paleoclimate studies: doi: 10.1002/2015GC006010. Received.

Kottmeier, D.M., Rokitta, S.D., Tortell, P.D., and Rost, B., 2014, Strong shift from HCO3- to CO2 uptake in Emiliania huxleyi with acidification: New approach unravels acclimation versus short-term pH effects: Photosynthesis Research, v. 121, p. 265–275, doi: 10.1007/s11120-014-9984-9.

Lambert, F., Tagliabue, A., Shaffer, G., Lamy, F., Wincklet, G., Farias, L., Gallardo, L., and Pol-Holz, R. De, 2015, Dust fluxes and iron fertilization in Holocene and Last Glacial Maximum climates: Geophysical Research Letters, v. 42, p. 6014–6023, doi: 10.1002/2015GL064250.Received.

Langmann, B., Zaksek, K., and Duggen, S., 2010, Volcanic ash as fertiliser for the surface ocean: Atmospheric Chemistry and Physics, v. 10, p. 3891–3899.

Landing, W.M., Shelley, R.U., Measures, C.I., Lao, Y., Ohnemus, D.C., Fleisher, M.Q., Hayes, C.T., Moran, S.B., Huang, K.-F., Robinson, L.F., Lam, P.J., Kadko, D., Lu, Y., Anderson, R.F., et al., 2016, How well can we quantify dust deposition to the ocean? Philosophical Transactions of the Royal Society A: Mathematical, Physical and Engineering Sciences, v. 374, p. 1–26, doi: 10.1098/rsta.2015.0285.

Lauderdale, J.M., Dutkiewicz, S., Williams, R.G., and Follows, M.J., 2016, Quantifying the drivers of ocean-atmosphere CO_2 fluxes: Global Biogeochemical Cycles, v. 30, p. 983–999, doi: 10.1002/2016GB005400.

Li, F., Vogelmann, A.M., and Ramanathan, V., 2004, Saharan dust aerosol radiative forcing measured from space: Journal of Climate, v. 17, p. 2558–2571, doi: 10.1175/1520-0442(2004)017<2558:SDARFM>2.0.CO;2.

Li, F., Ginoux, P., and Ramaswamy, V., 2008, Distribution, transport, and deposition of mineral dust in the Southern Ocean and Antarctica: Contribution of major sources: Journal of Geophysical Research, v. 113, p. 1–15, doi: 10.1029/2007JD009190.

Lindsay, W.L., 1991, Iron oxide solubilization by organic matter and its effect on iron availability: Plant and Soil, v. 130, p. 27–34.

Longhurst, A.R., and Glen Harrison, W., 1989, The biological pump: Profiles of plankton production and consumption in the upper ocean: Progress in Oceanography, v. 22, p. 47–123, doi: 10.1016/0079-6611(89)90010-4.

Mahowald, N., 2011, Aerosol Indirect Effect on Biogeochemical Cycles and Climate: v. 334, p. 794–796, doi: 10.1016/S1135-2523(12)60093-8.

Mann, E.L., Ahlgren, N., Moffett, J.W., and Chisholm, S.W., 2002, Copper toxicity and cyanobacteria ecology in the Sargasso Sea: Limnology and Oceanography, v. 47, p. 976–988.

Martin, J.H., and Fitzwater, S.E., 1988, Iron deficiency limits phytoplankton growth in the north-east pacific subarctic: Nature, v. 331, p. 341–343, doi: 10.1038/331341a0.

Martin, E., 2018, Volcanic Plume Impact on the Atmosphere and Climate: O- and S-Isotope Insight into Sulfate Aerosol Formation: Geosciences, v. 8, p. 198, doi: 10.3390/geosciences8060198.

Martínez-García, A., Sigman, D.M., Ren, H., Anderson, R.F., Straub, M., Hodell, D.A., Jaccard, S.L., Eglinton, T.I., and Haug, G.H., 2014, Iron fertilization of the subantarctic ocean during the last ice age: Science, v. 343, p. 1347–1350, doi: 10.1126/science.1246848.

McDowell Group, Alaska Seafood Marketing Institute, 2015, The Economic Value of Alaska's Seafood Industry: p. 1–32.

Mehra, O.P., and Jackson, M.L., 1958, Iron Oxide Removal from Soils and Clays by a Dithionite-Citrate System Buffered with Sodium Bicarbonate: Clays and Clay Minerals, v. 7, p. 317–327, doi: 10.1346/CCMN.1958.0070122.

Miklasz, K.A., and Denny, M.W., 2010, Diatom sinking speeds: Improved predictions and insight from a modified Stoke's law: Limnology and Oceanography, v. 55, p. 2513–2525, doi: 10.4319/lo.2010.55.6.2513.

Miller, R.L., Tegen, I., and Perlwitz, J., 2004, Surface radiative forcing by soil dust aerosols and the hydrologic cycle: Journal of Geophysical Research: Atmospheres, v. 109, doi: 10.1029/2003JD004085.

Moore, J.K., Doney, S.C., Glover, D.M., and Fung, I.Y., 2002, Iron cycling and nutrient-limitation patterns in surface waters of the world ocean: Deep-Sea Research Part II: Topical Studies in Oceanography, v. 49, p. 463–507, doi: 10.1016/S0967-0645(01)00109-6.

Moore, D.M., and Reynolds, R.C., 1989, X-ray diffraction and the identification and analysis of clay minerals: Oxford University Press.

Morel, F.M.M., Rueter, J.G., and Price, N.M., 1991a, Iron nutrition of phytoplankton and its possible importance in the ecology of ocean regions with high nutrient and low biomass: Oceanography, v. 4, p. 56–61, doi: 10.5670/oceanog.1991.03.

Morel, F.M.M., Hudson, R.J.M., and Price, N.M., 1991b, Limitation of productivity by trace metals in the sea: Limnology and Oceanography, v. 36, p. 1742–1755, doi: 10.4319/lo.1991.36.8.1742.

Morel, F.M.M., 1999, Opportunities for Environmental Applications of Marine Biotechnology Proceedings: Washington, D.C., National Academy Press, 96 p.

Müller, J., Romero, O., Cowan, E.A., McClymont, E.L., Forwick, M., Asahi, H., März, C., Moy, C.M., Suto, I., Mix, A., and Stoner, J., 2018, Cordilleran ice-sheet growth fueled primary productivity in the Gulf of Alaska, northeast Pacific Ocean: Geology, v. 46, p. 307–310, doi: 10.1130/G39904.1.

Neff, P.D., and Bertler, N.A.N., 2015, Journal of Geophysical Research: Atmospheres: v. 120, p. 9303–9322, doi: 10.1002/2015JD023304.Received.

Olgun, N., Duggen, S., Croot, P.L., Delmelle, P., Dietze, H., Schacht, U., Óskarsson, N., Siebe, C., and Auer, A., 2011, Surface ocean iron fertilization: The role of airborne volcanic ash from subduction zone and hot spot volcanoes and related iron fluxes into the Pacific Ocean: Global Biogeochemical Cycles, v. 25, p. 1–15, doi: 10.1029/2009GB003761.

Okin, G.S., Mahowald, N., Chadwick, O.A., and Artaxo, P., 2004, Impact of desert dust on the biogeochemistry of phosphorus in terrestrial ecosystems: Global Biogeochemical Cycles, v. 18, doi: 10.1029/2003GB002145.

Paytan, A., Mackey, K.R.M., Chen, Y., Lima, I.D., Doney, S.C., Mahowald, N., Labiosa, R., and Post, A.F., 2009, Toxicity of atmospheric aerosols on marine phytoplankton: Proceedings of the National Academy of Sciences, v. 106, p. 4601–4605.

Penner, J.E., Hegg, D., and Leaitch, R., 2001, Unraveling the Role of Aerosols in Climate Change: Environmental Science and Technology, v. 35, p. 332–340 A, doi: 10.1021/es0124414.

Poulton, S.W., and Canfield, D.E., 2005, Development of a sequential extraction procedure for iron: Implications for iron partitioning in continentally derived particulates: Chemical Geology, v. 214, p. 209–221, doi: 10.1016/j.chemgeo.2004.09.003.

Poulton, S.W., and Raiswell, R., 2005, Chemical and physical characteristics of iron oxides in riverine and glacial meltwater sediments: Chemical Geology, v. 218, p. 203–221, doi: 10.1016/j.chemgeo.2005.01.007.

Prospero, J.M., 1999, Long-range transport of mineral dust in the global atmosphere : Impact of African dust on the environment of the southeastern United States: Proceedings of the National Academy of Sciences, v. 96, p. 3396–3403.

Raes, F., Dingenen, R. Van, Vifnati, E., Wilson, J., Putaud, J.-P., Seinfeld, J.H., and Adams, P., 2000, Formation and cycling of aerosols in the global troposphere: Atmospheric Environment Millenial Review, v. 34, p. 4215–4240, doi: 10.1016/S1352-2310(00)00239-9.

Ramanathan, V., Crutzen, P.J., Kiehl, J.T., and Rosenfeld, D., 2001, Aerosols, Climate, and the Hydrological Cycle: Science, v. 294, p. 2119–2125.

Raven, J.A., Evans, M.C.W., and Korb, R.E., 1999, The role of trace metals in photosynthetic electron transport in O2-evolving organisms: Photosynthesis Research, v. 60, p. 111–149.

Rea, D.K., 1994, The Paleoclimate Record Provided By Eolian Deposition in the Deep Sea: Reviews of Geophysics, v. 32, p. 159–195.

Richardson, T.L., and Jackson, G.A., 2007, Small Phytoplankton and Carbon Export from the Surface Ocean: Science, v. 315, p. 838–840.

Robock, A., 2000, Volcanic Eruptions and Climate: Reviews of Geophysics, v. 38, p. 191–219.

Rodhe, H., Charlson, R., and Crawford, E., 1998, Svante Arrhenius and the Greenhouse Effect In Context: Royal Swedish Academy of Sciences, v. 26, p. 13–20.

Rue, E.L., and Bruland, K.W., 1995, Complexation of iron(III) by natural organic ligands in the Central North Pacific as determined by a new competitive ligand equilibration/adsorptive cathodic stripping voltammetric method: Marine Chemistry, v. 50, p. 117–138, doi: 10.1016/0304-4203(95)00031-L.

Schiebel, R., 2002, Planktic foraminiferal sedimentation and the marine calcite budget: Global Biogeochemical Cycles, v. 16, p. 13-1 through 13-21, doi: 10.1029/2001GB001459.

Schoffman, H., Lis, H., Shaked, Y., and Keren, N., 2016, Iron–Nutrient Interactions within Phytoplankton: Frontiers in Plant Science, v. 7, p. 1–12, doi: 10.3389/fpls.2016.01223.

Schuur, E.A.G., Trumbore, S.E., Druffel, E.R.M., Southon, J.R., Steinhof, A., Taylor, R.E., and Turnbull, J.C., 2016, Radiocarbon and the Global Carbon Cycle, *in* Schuur, E.A.G., Druffel, E., and Trumbore, S.E. eds., Radiocarbon and Climate Change: Mechanisms, Applications and Laboratory Techniques, Cham, Springer International Publishing, p. 1–19, doi: 10.1007/978-3-319-25643-6_1.

Schroth, A.W., Crusius, J., Sholkovitz, E.R., and Bostick, B.C., 2009, Iron solubility driven by speciation in dust sources to the ocean: Nature Geoscience, v. 2, p. 337–340, doi: 10.1038/ngeo501.

Serno, S., Winckler, G., Anderson, R.F., Hayes, C.T., McGee, D., Machalett, B., Ren, H., Straub, S.M., Gersonde, R., and Haug, G.H., 2014, Eolian dust input to the Subarctic North Pacific: Earth and Planetary Science Letters, v. 387, p. 252–263, doi: 10.1016/j.epsl.2013.11.008.

Shao, Y., Wyrwoll, K.H., Chappell, A., Huang, J., Lin, Z., McTainsh, G.H., Mikami, M., Tanaka, T.Y., Wang, X., and Yoon, S., 2011, Dust cycle: An emerging core theme in Earth system science: Aeolian Research, v. 2, p. 181–204, doi: 10.1016/j.aeolia.2011.02.001.

Shoenfelt, E.M., Sun, J., Winckler, G., Kaplan, M.R., Borunda, A.L., Farrell, K.R., Moreno, P.I., Gaiero, D.M., Recasens, C., Sambrotto, R.N., and Bostick, B.C., 2017, High particulate iron(II) content in glacially sourced dusts enhances productivity of a model diatom: Science Advances, v. 3, p. 1–10, doi: 10.1126/sciadv.1700314.

Siegel, D.A., Buesseler, K.O., Doney, S.C., Sailley, S.F., Behrenfeld, M.J., and Boyd, P.W., 2014, Global assessment of ocean carbon export by combining satellite observations and food-web models: Global Biogeochemical Cycles, v. 28, p. 181–196, doi: 10.1002/2013GB004743.

Sigman, D.M., Hain, M.P., and Haug, G.H., 2010, The polar ocean and glacial cycles in atmospheric CO_2 concentration: Nature, v. 466, p. 47–55, doi: 10.1038/nature09149.

Spirakis, C.S., 1991, Iron fertilization with Volcanic Ash?: Eos, v. 72, p. 331–342, doi: 10.1166/Jnn.2007.460.

Steinberg, D.K., Carlson, C.A., Bates, N.R., Goldthwait, S.A., Madin, L.P., and Michaels, A.F., 2000, Zooplankton vertical migration and the active transport of dissolved organic and inorganic carbon in the Sargasso Sea: Deep-Sea Research Part I, Oceanographic Research Papers, v. 47, p. 137–158, doi: 10.1016/S0967-0637(99)00052-7.

Stephens, G.L., Tsay, S.-C., and Jr., Stackhouse, P.W., 1990, The Relevance of the Microphysical and Radiative Properties of Cirrus Clouds to Climate and Climatic Feedback: Journal of the Atmospheric Sciences, v. 47, p. 1742–1753.

Stock, C.A., John, J.G., Rykaczewski, R.R., Asch, R.G., Cheung, W.W.L., Dunne, J.P., Friedland, K.D., Lam, V.W.Y., Sarmiento, J.L., and Watson, R.A., 2017, Reconciling fisheries catch and ocean productivity: Proceedings of the National Academy of Sciences, v. 114, p. E1441–E1449, doi: 10.1073/pnas.1610238114.

Tegen, I., and Fung, I., 1994, Modeling of mineral dust in the atmosphere: Sources, transport, and optical thickness: Journal of Geophysical Research, v. 99, p. 22897–22914, doi: 10.1029/94JD01928.

Tegen, I., Werner, M., Harrison, S.P., and Kohfeld, K.E., 2004, Relative importance of climate and land use in determining present and future global soil dust emission: Geophysical Research Letters, v. 31, p. 1–3, doi: 10.1029/2004GL021272.

Trapp, J.M., Millero, F.J., and Prospero, J.M., 2010, Trends in the solubility of iron in dust-dominated aerosols in the equatorial Atlantic trade winds: Importance of iron speciation and sources: Geochemistry, Geophysics, Geosystems, v. 11, p. 1–22, doi: 10.1029/2009GC002651.

Twining, B.S., Baines, S.B., Bozard, J.B., Vogt, S., Walker, E.A., and Nelson, D.M., 2011, Metal quotas of plankton in the equatorial Pacific Ocean: Deep-Sea Research Part II: Topical Studies in Oceanography, v. 58, p. 325–341, doi: 10.1016/j.dsr2.2010.08.018.

USGS, 2016, Available Powdered Reference Materials: USGS Geochemical Reference Materials and Certificates, https://crustal.usgs.gov/geochemical_reference_standards/powdered_RM.html.

Visser, F., Gerringa, L.J.A., Van Der Gaast, S.J., De Baar, H.J.W., and Timmermans, K.R., 2003, The role of the reactivity and content of iron of aerosol dust on growth rates of two Antarctic diatom species: Journal of Phycology, v. 39, p. 1085–1094, doi: 10.1111/j.0022-3646.2003.03-023.x.

Wang, Y.Q., Zhang, X.Y., and Draxler, R.R., 2009, TrajStat: GIS-based software that uses various trajectory statistical analysis methods to identify potential sources from long-term air pollution measurement data: Environmental Modelling and Software, v. 24, p. 938–939, doi: 10.1016/j.envsoft.2009.01.004.

Wang, Y., Zhang, H., Chen, H., and Chai, F., 2018, The sources and transport of iron in the North Pacific and its impact on marine ecosystems: Atmospheric and Oceanic Science Letters, v. 12, p. 30–34, doi: 10.1080/16742834.2019.1545513.

Wu, J., Boyle, E., Sunda, W., and Wen, L., 2001, Soluble and Colloidal Iron in the Oligotrophic North Atlantic and North Pacific: Science, v. 293, p. 847–850.

Whitney, P.R., 1975, Relationship of manganese-iron oxides and associated heavy metals to grain size in stream sediments: Journal of Geochemical Exploration, v. 4, p. 251–263, doi: 10.1016/0375-6742(75)90005-9.

Zdanowicz, C.M., Zielinski, G.A., and Wake, C.P., 1998, Characteristics of modern atmospheric dust deposition in snow on the Penny Ice Cap, Baffin Island, Arctic Canada: Tellus B: Chemical and Physical Meteorology, v. 50, p. 506–520, doi: 10.3402/tellusb.v50i5.16234.

Appendix I. Fractional Iron Solubility. MilliQ leach data.

Sample ID	***Volume (mL)***	**Replicate 1 (%)**	**Replicate 2 (%)**	**Replicate 3 (%)**	**Replicate 4 (%)**	**Average FeS (%)**	**Standard Deviation**	**Cumulative Solubility (FeS, %)**
AT-3982	1000	0.008	0.010	0.014		0.011	0.003	0.060
AT-3982	500	0.010	0.026	0.015		0.017	0.008	0.050
AT-3982	250	0.008	0.005	0.050		0.021	0.025	0.032
AT-3982	100	0.009	0.019	0.006		0.011	0.007	0.007
AK2016-08	1000	0.037	0.030	0.033		0.033	0.003	0.147
AK2016-08	500	0.038	0.040	0.024		0.034	0.008	0.113
AK2016-08	250	0.039	0.026	0.026		0.030	0.007	0.031
AK2016-08	100	0.075	0.027	0.045		0.049	0.024	0.024
AK2016-05	1000	0.074	0.011	0.016	0.016	0.034	0.030	0.320
AK2016-05	500	0.154	0.026	0.019	0.019	0.066	0.067	0.286
AK2016-05	250	0.205	0.055	0.022	0.022	0.094	0.088	0.198
AK2016-05	100	0.263	0.085	0.030	0.030	0.126	0.111	0.111
AK2016-12	1000	0.038	0.049	0.193		0.093	0.087	0.430
AK2016-12	500	0.029	0.029	0.299		0.119	0.156	0.337
AK2016-12	250	0.035	0.041	0.224		0.100	0.107	0.236
AK2016-12	100	0.049	0.038	0.266		0.118	0.129	0.129
AK2016-18	1000	0.028	0.051	0.045		0.041	0.012	0.206
AK2016-18	500	0.034	0.047	0.039		0.040	0.006	0.165
AK2016-18	250	0.039	0.037	0.046		0.041	0.005	0.017
AK2016-18	100	0.099	0.078	0.076		0.084	0.013	0.013

Appendix II. Sample locations and descriptions

Sample ID	Latitude (N)	Longitude (W)	Description
AK2016-01	62˚ 19.389’	150˚ 07.311’	Clay to fine sand within sand-gravel bank. Collected downstream of Susitna River and Talkeetna River confluence.
AK2016-02	62˚ 19.615’	150˚ 07.272’	Fine grained sediment collected from the Susitna river bank.
AK2016-03	61˚ 30.152’	149˚ 01.836’	Silt from flat area next to a big eddy on the Knik River. Topography very steep in mountains, wide/broad river valley.
AK2016-04	61˚ 36.344’	149˚ 04.256’	Sediment from large sand/gravel bar of Matanuska river. Below bedrock narrows.
AK2016-05	61˚ 47.719’	147˚ 47.940’	Silt ripples in damp side channel of the Matanuska river, collected ~0.5 mi below glacier terminus.
AK2016-06	62˚ 36.136’	144˚ 38.632’	Chistochina river left, upstream bridge of AK Hwy 1 (ToK Highway). Fine grained sed near puddle in braided streambed. River has vegetated gravel bars and lots of driftwood. Many channels, no whitewater. Drain Eastern Alaska Range.
AK2016-07	62˚ 39.673’	144˚ 28.228’	Loess from N of Hwy 1 near mile 43, can see primary bedding features, fine layering at the top of the outcrop. Tree roots present to small degree in smapled section, more abundant above. At least 0.5-1 m intact loess with layering, but probably multiple meters. Overall outcrop ~35 ft tall down to road level. "Tastes great". Very powdery.
AK2016-08	62˚ 38.297’	144˚ 31.588’	Copper river side channel above Chistochina river confluence. Mile 40 easement 0.3 miles from Rd. Can't quite see main channel. But can see a volcano. Spooked ptarmigan.
AK2016-10	62˚ 18.157’	145˚ 18.386’	Gakona river upstream Hwy 1 bridge. Narrow slightly braided channel. Below massive gravel/loess deposit. Drains AK range.
AK2016-11	61˚ 32.081	144˚ 22.720’	Chitina loess section E of Copper river, S of Chitina river, within paleosol complex. Approx. 1m above contact with diamicton. Found gastropods at top of paleosol complex.
AK2016-12	61˚ 32.081	144˚ 22.720’	Chitina loess section E of Copper river, S of Chitina river. Light-colored above paleosol complex, potential ash. ~1.2m above contact with diamicton.

AK2016-13	61˚ 32.081’	144˚ 22.720’	Chitina loess section E of Copper river, S of Chitina river, halfway up section, within stump layer. Silt immediately surrounding stump.
AK2016-14	61˚ 32.081’	144˚ 22.720’	Chitina loess section E of Copper river, S of Chitina river, near top of section. Primary layering visible, in site stumps present, sampling beneath overhang ~1m from top of section, ~100m down road from samples 11-13 (moved for better access to top layers). Sample taken beneath ancient looking stump.
AK2016-16	62˚ 32.317’	145˚ 20.576’	Loess above Chitna, North side of river, way above bank. Road cut loess directly atop bedrock. Layering with gray-tan-brown colored bands. Loess with potential paleosol at base, directly on limestone bedrock. No rocks present, gastropods are present, as well as some in situ stumps ~1m from the surface. Atop bedrock, 1.25 m above sample 15, about 90 cm below the soil surface and right below an in situ stump.
AK2016-17	61˚ 31.310’	144˚ 25.163’	Copper river silty sand from side channel right, below bridge near nice silt deposit. Middle of salmon dip-netting season, so very crowded with campers and people.
AK2016-18	61˚ 47.294’	148˚ 26.830’	Matanuska valley roadcut loess. W of pass near glacier. Layering visible. Seds above bedrock. ~1.5m of seds pass over ~1m of till or river gravel, then bedrock. Sampled far right side of outcrop b/c difficult to climb crumbling bedrock.
YT2017-PS02	61.002842˚	138.495105˚	Collected near Kluane Lake in the Yukon Territory.
AT-3982	59˚ 46.445’	151˚ 36.394’	Bulk sample, collected on clean poster board set out to collect ash, 48"x60" collected 7:20-7:50AM, 1 mm of ash pristine sample (never wetted).
AT-3680	56.0008˚	161.20485˚	Pristine dry (never wetted) ash fall from 3/28/16 ash fall in Nelson Lagoon collected off wood planks of a porch within hours of the 3/28/16 fallout (3000 grams).